European Journal of Organic Chemistry

Supporting Information

Structure-Based Design and in-Flow Synthesis of Aromatic Endoperoxides Acting as Oxygen Releasing Agents

Marco Agnes,* Adelaide Santagata, Daniele Veclani, Alessandro Venturini, Magda Monari, Paolo Dambruoso, and Ilse Manet*

Table of contents

1. Materials and methods

General. *Tetrakis* (triphenylphosphine)palladium (0) ($Pd(PPh_3)_4$, CAS: 14221-01-3, 98%) and caesium carbonate (Cs_2CO_3, CAS: 534-17-8, 99%) were purchased from *Fluorochem* and used as received. 9,10-Dibromoanthracene (DBA, CAS: 523-27-3, ≥98%), 2-propyn-1-ol (CAS: 107-19-7, propargyl alcohol, >98.0%) were purchased from *Tokyo Chemical Industry* (TCI) and used as received. 5,10,15,20-*Tetrakis*(3-hydroxyphenyl)porphyrin (mTHPP, CAS: 22112-79-4, 95%) was purchased from *BLDpharm* and used as received. *Bis*(triphenylphosphine)palladium(II) dichloride ($Pd(PPh_3)_2Cl_2$, CAS: 13965-03-2, 98%), copper(I) iodide (CuI, CAS: 7681-65-4, 98%), di*iso*propylamine (CAS: 108-18-9, > 99%), lithium hydroxide (LiOH, CAS: 1310-65-2), 4-fluorophenylboronic acid (FPBA, CAS 1765-93-1, ≥95%), sodium sulfate anhydrous (Na_2SO_4, CAS: 7757-82-6, >99%), Methylene blue (C.I.52015) trihydrate for microscopy Certistain (MB, CAS 7220-79-3), thin layer chromatography (TLC) aluminium plates coated with silica gel/fluorescent indicator, molecular sieves (4 Å, CAS: 70955-01-0), silica gel (SiO_2, 40-63 µm, 200 mesh, CAS: 112926-00-8) and all solvents (analytical or Uvasol® grade) were purchased from Sigma-Aldrich and used as received. Deuterated solvents (DMSO-d_6 99.90%, and $CDCl_3$ 99.96%) were purchased from Eurisotop and used as received.

Photooxygenation reactions. Continuous-flow experiments were performed with a Vapourtec *Ltd.* easy-Photochem E-Series system (**Figure S1**) equipped with a UV-150 photochemical reactor kit in combination with a high-power LED emitting light at 525 nm wavelength, V-3 pumps and cryogenic reaction kit. See below for the followed synthetic procedure.

Figure S1: Vapourtec *Ltd.* easy-Photochem E-Series system used for the photochemical step of the reaction.

***NMR spectroscopy*.** NMR spectra were recorded on an Agilent DD2 spectrometer operating at 500 MHz for ^{1}H and 125 MHz for ^{13}C, or on a Varian Mercury 400 MHz for ^{1}H and 100 MHz for ^{13}C, equipped with a broadband probe, using the pulse sequences provided by the library of the instrument (software Agilent VnmrJ 4.2). The assignment of the peaks in the ^{1}H and ^{13}C NMR spectra was accomplished using 2D ^{1}H-^{1}H COSY, ^{1}H-^{13}C HSQC, ^{1}H-^{13}C HMBC and 2D ROESY NMR experiments. All NMR spectra were processed with MestreNova 14.2.0.

***ESI-MS spectrometry*.** ESI-MS analysis were performed by direct injection of acetonitrile or methanol solutions of the compounds using a WATERS ZQ 4000 mass spectrometer.

***Spectroscopic measurements*.** For the monitoring of the photooxygenation reactions and stability of the endoperoxides, absorption spectra were recorded on a Perkin-Elmer Lambda 950 spectrophotometer. 0.1 cm cuvettes were used and Uvasol® solvents were used as reference.
For the monitoring of the cycloreversion, absorption spectra were recorded on an Agilent Cary 100 UV-Vis spectrophotometer equipped with a multicell peltier accessory allowing accurate control of the temperature. The *Scan* and *Scanning Kinetics* applications were chosen among the library of Cary WinUV software. 1.0 cm cuvettes were used and Uvasol® solvents were used as reference. See below for the detailed experimental procedure.

Kinetic data analysis. UV-vis spectra in DMSO were collected at different times heating the solutions at the selected temperatures. Absorbance was read at 378 nm for **PCPA** and **PFPA** and at 388 nm for **DIPA** and corrected for the constant contribution of mTHPP. The increase in absorbance was used to calculate the amount of EPO converting to the parent compound. The natural logarithm of the normalized EPO concentration was plotted vs time to obtain the rate constant. The latter constant at different temperatures was used to prepare Arrhenius plots of ln(k) vs 1/T affording the activation energy E_a as slope. The equation $t_{1/2} = \ln(2)/ k$ was used to obtain the half-lives of the EPOs at selected temperatures.

Computational studies. Density functional theory (DFT) calculations were carried out using the B.01 revision of Gaussian 16 program package.[1] B3LYP hybrid functional[2–5] was employed in combinations with Def2-TZVP basis set for all atoms[6,7]; the efficacy of such computational protocol has already been validated on similar studies reported in literature.[8–10] Due to the key role of solvation in influencing the thermodynamic parameters in organic molecules reactivity,[11–13] environmental effects have been introduced by representing dichloromethane as a polarizable

continuum method (PCM).[14] All systems investigated were fully optimized in PCM solvent without symmetry constraints. In order to confirm that stationary points were actually minima geometries, the analytical calculation of second derivatives of the energy and vibrational frequency analysis were carried out.

The dissociation energy (E_{diss}) for a two-body system, is defined in eq. 1

$$\mathbf{E_{diss} = (E_R + E_{O2}) - E_{OX} + BSSE} \qquad \mathbf{eq.1}$$

In eq. E_{OX} is the total energy of the endoperoxide molecule, E_R is the energy of the organic subtract and E_{O2} is the energy of the singlet oxygen ($^1O_2$) species. All E_{diss} were corrected by adding the basis set superposition error (BSSE) using the counterpoise method by Boys and Bernardi.[15]

Non-Covalent Interactions (NCI) analysis[16,17] was used to obtained a clear picture of non-covalent interaction in molecules investigated. NCI is based on the density (ρ) and its derivatives, in particular, the identification of the non-covalent interaction is based on the spikes that appear in the reduced density gradient (RDG) at low densities. However, such interaction is both favourable and unfavourable, to discriminate and between them the sign of the second density Hessian eigenvalue (λ_2) times the density (sign(λ_2)ρ) is used as follow:

- Attractive interaction → $\lambda_2 < 0$;
- Repulsive interaction → $\lambda_2 > 0$;
- Weak van der Waals interactions by $\lambda_2 \approx 0$

A better visualization of these interactions was obtained with the constructions of colored 3D surfaces based on sign(λ_2)ρ values: blue for strong attractive interactions ($\lambda_2 < 0$), green for weak van der Waals interactions ($\lambda_2 \approx 0$) and red for strong repulsive interactions ($\lambda_2 > 0$).

X-ray crystallography. Single crystals of **PNBA**, **ANBA**, **PABA**, **PABA-O2** and **PFPA** were obtained from slow evaporation of different mixtures of solvents/antisolvents, namely THF : DCM, ethyl ether : acetone : toluene, THF : EtOH(aq.). Single crystals of **NABA** were obtained from slow evaporation of the mixture ethyl ether : acetone : toluene and were found to match previously published data,[18] following powder diffraction analysis (**Figure S2**).

The X-ray intensity data were collected on a Bruker APEX-II CCD diffractometer using Mo−Kα (**ANBA**, **PABA**, **PNBA**, **PFPA**) or Cu-Kα radiation (**PABA-O2**). All data were processed using the Bruker suite of programs[19–21] and the structures were solved by direct methods and refined with the SHELX program suite.[22,23] All non-hydrogen atoms were assigned anisotropic displacement parameters. Most of the hydrogen atoms were located in the Fourier map, placed in idealized positions and

included as riding with constrained isotropic displacement parameters (C—H = 0.98, 0.99 and 0.93 Å) for methyl, methylene and aromatic protons, respectively, and refined as riding with Uiso(H) = 1.2 or 1.5Ueq(C). In **PNBA** there are six independent molecules. In the asymmetric unit of **PABA-O2** there is one THF molecule. In **ANBA**, **PABA** and **PFPA** disordered solvent molecules that could not be identified and modelled were observed and the remaining electron density had its contribution to the diffraction data accounted for with the SQUEEZE routine within PLATON.[24] Analysis of the solvent accessible voids from Squeeze results in a total electron count of 198, 120 and 283 e^- within the voids per unit cell, with a void volume of 947.1(25.6%), 534.6(12.6%) and 1257.7(16.2%) $Å^3$ for **ANBA**, **PABA** and **PFPA**, respectively. **Table S1** reports crystal data and refinement parameters obtained from the crystals whose molecular graphics and drawings were generated using the program Mercury.[25]

Crystallographic data have been deposited with the Cambridge Crystallographic Data Centre (CCDC) as supplementary publication number CCDC 2351990-2351994. Copies of the data can be obtained free of charge via www.ccdc.cam.ac.uk/getstructures.

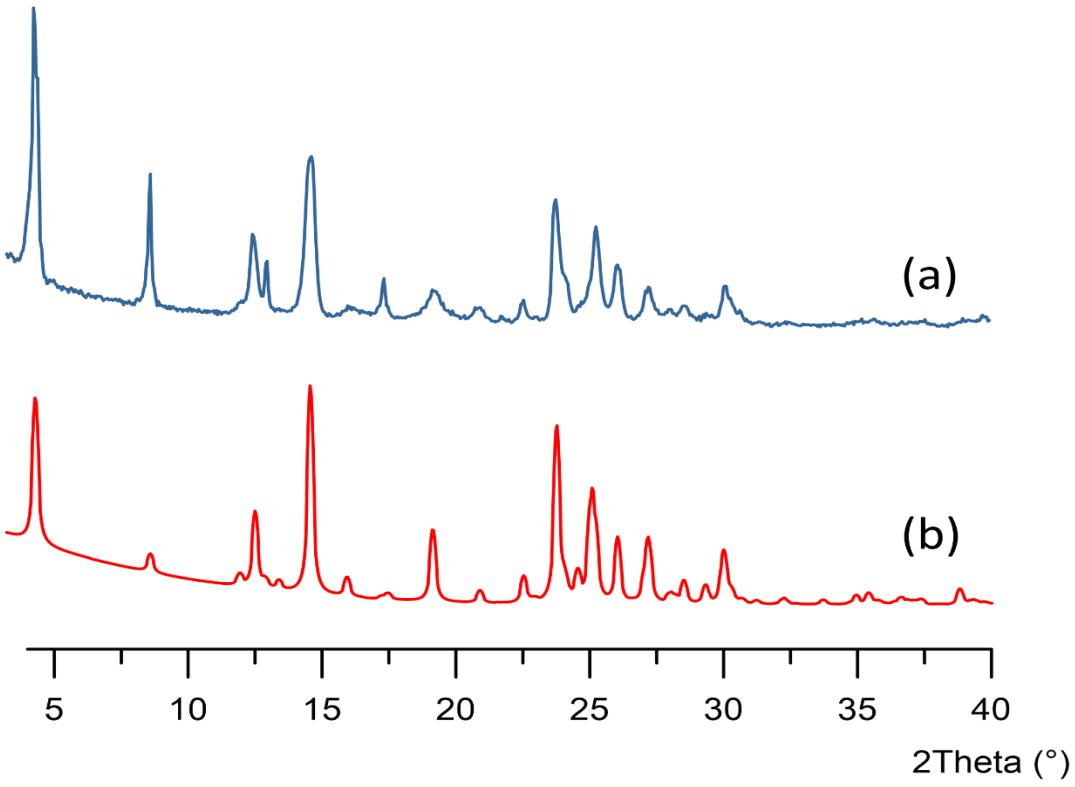

Figure S2: (a) X-ray diffraction pattern of **NABA** sample; (b) Calculated pattern of **NABA** from single crystal data: since literature data were collected at low temperature,[18] peak positions are fitted to experimental positions in order to get lattice parameters of the sample *a*= 3.998(1) Å; *b*= 41.13(1); Å *c*= 7.638(1) Å; β= 99.45(1)° compared to experimental ones (ochre line, Cu radiation, calculated parameters: a= 3.998(1) Å; b= 41.13(1) Å; c= 7.638(1) Å; β= 99.45(1)°).

Table S1. Crystal data and experimental details for **ANBA**, **PABA**, **PABA-O2**, **PNBA** and **PFPA**.

Compound	***ANBA***	***PABA***	***PABA-O2***	***PNBA***	***PFPA***
Formula	$C_{21}H_{14}O_2$	$C_{27}H_{18}O_2$	$C_{27}H_{18}O_4.C_4H_8O$	$C_{23}H_{16}O_2$	$C_{23}H_{15}FO$
Fw, g/mol	298.32	374.41	478.52	324.36	326.35
T, K	296(2)	296(2)	100(2)	296(2)	296(2)
λ, Å	0.71073	0.71073	1.54178	0.71073	0.71073
Crystal symmetry	Monoclinic	Orthorhombic	Monoclinic	Triclinic	Monoclinic
Space group	C2/c	Pbcn	$P2_1/c$	P-1	C2/c
a, *Å*	17.1124(7)	53.067(4)	13.3937(16)	15.6086(6)	43.069(3)
b, *Å*	7.6476(3)	9.7368(8)	10.8248(12)	18.0307(7)	9.0877(6)
c, *Å*	28.9239(12)	8.2195(6)	16.429(2)	19.9482(7)	22.4141(16)
α, °	90	90	90	64.632(1)	90
β,°	102.447(1)	90	101.412(5)	74.849(1)	117.793(2)
γ, °	90	90	90	82.962(1)	90
Cell volume, Å³	3696.3(3)	4247.0(5)	2334.8(5)	4896.1(3)	7760.7(9)
Z	8	8	4	12	16
D_c, *Mg m⁻³*	1.072	1.171	1.361	1.320	1.117
μ(Mo-K_α), *mm⁻¹*	0.068	0.073	0.741	0.083	0.074
F(000)	1248	1568	1008	2040	2720
Crystal size/ mm	0.20 x 0.15 x 0.10	0.20 x 0.15 x 0.07	0.10 x 0.10 x 0.06	0.23 x 0.15 x 0.10	0.25 x 0.20 x 0.10
ϑ limits, °	2.438 to 24.997	2.303 to 22.993	4.923 to 68.550	1.663 to 28.344	1.821 to 24.997
Reflections collected	27928	37069	39025	78867	45744
Unique obs. Reflections [$F_o > 4\sigma(F_o)$]	3214 [R(int) = 0.0427]	2847 [R(int) = 0.1110]	4268 [R(int) = 0.0683]	24206 [R(int) = 0.0394]	6723 [R(int) = 0.0696]
Goodness-of-fit-on F^2	1.030	1.117	1.103	1.149	1.113
$R_1(F)^a$, $wR_2(F^2)$ $[I > 2\sigma(I)]^b$	0.0411, 0.0998	0.1052, 0.2126	0.0762, 0.2300	0.0556, 0.1581	0.0911, 0.2028
Largest diff. peak and hole, e. Å⁻³	0.228 and -0.278	0.202 and -0.330	0.448 and -0.869	0.434 and -0.356	0.328 and -0.306

[a] $R_1 = \Sigma||F_o|-|F_c||/\Sigma|F_o|$. [b] $wR_2 = [\Sigma w(F_o^2-F_c^2)^2/\Sigma w(F_o^2)^2]^{1/2}$
where $w = 1/[\sigma^2(F_o^2) + (aP)^2 + bP]$
where $P = (F_o^2 + F_c^2)/3$.

2. Supporting table and figures

Table S2: Computational analysis of anthracene derivatives: chemical structures and calculated dissociation energies (E_{diss}, kcal·mol^{-1}), ionization potentials (IP, eV) and electron affinities (EA, eV).

nr	Mol	E_{diss}	IP	EA	nr	Mol	E_{diss}	IP	EA
1	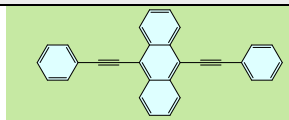	0.88	5.388	2.749	10	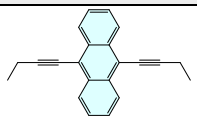	3.77	5.436	2.470
2	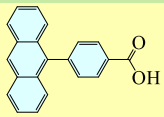	12.16	5.680	2.159	11	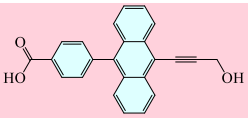	6.75	5.677	2.454
3	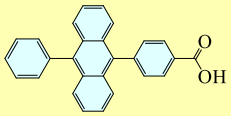	10.44	5.629	2.157	12	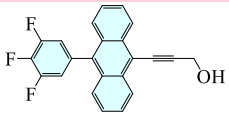	6.76	5.692	2.468
4	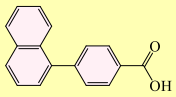	-3.49	6.198	1.981	13	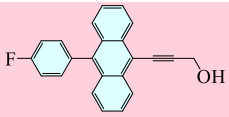	6.98	5.622	2.398
5	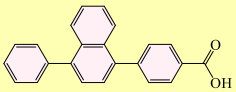	-4.31	6.082	1.996	14	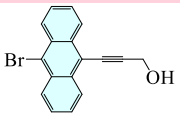	8.30	5.712	2.552
6	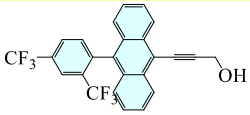	-0.98	5.702	2.485	15	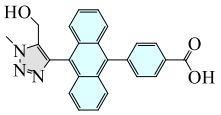	10.89	5.724	2.259
7	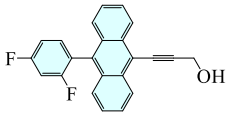	2.47	5.659	2.437	16	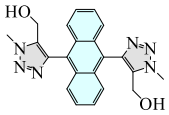	11.37	5.708	2.256
8	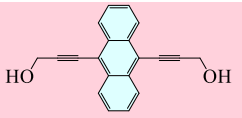	3.16	5.588	2.619	17	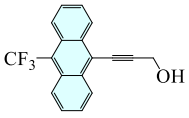	11.69	5.860	2.690
9	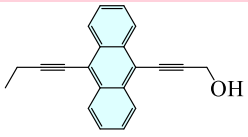	3.46	5.523	2.555	18	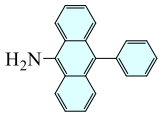	16.28	5.102	1.925

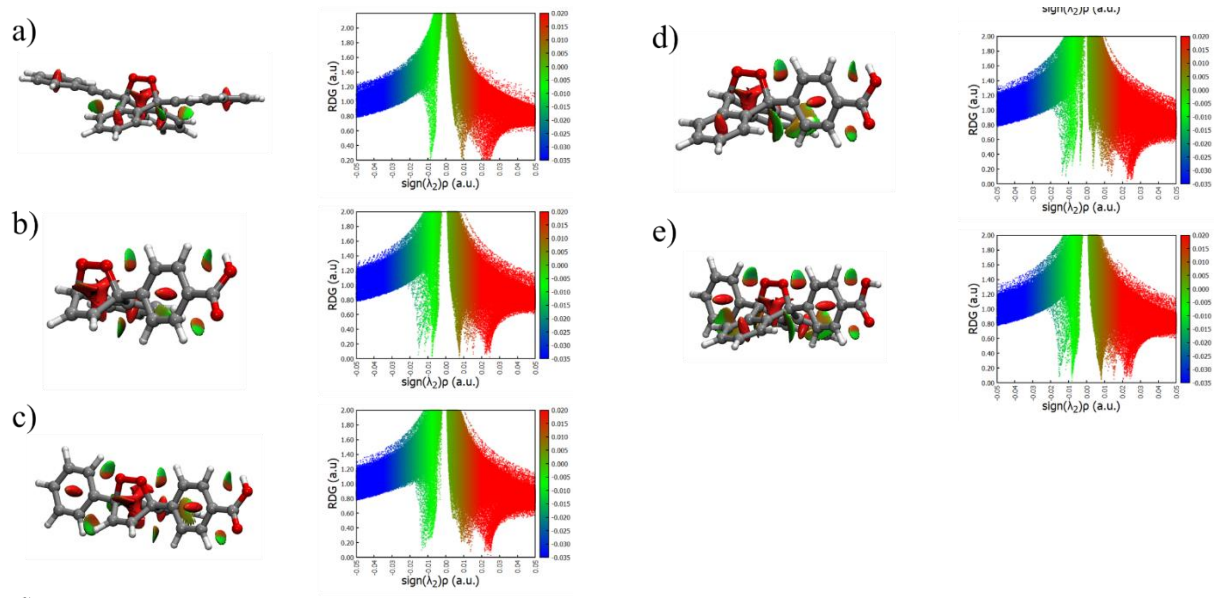

Figure S3: Reduced gradient density (RGD) 3D (isovalues 0.65) and 2D graphs of a) DPAA-O2, b) NABA-O2, c) PNBA-O2, d) ANBA-O2, e) PABA-O2. The sign of the product of λ_2 and ρ (sign(λ_2)ρ) is related with non-covalent interactions. Negative (sign(λ_2)ρ) value is the attractive part of the VdW interactions (green points); low positive value of (sign(λ_2)ρ) is the repulsive part of VdW interactions (brown points); high positive (sign(λ_2)ρ) value are related to the steric effect (red points).

Intense spikes at -0.010 sign(λ2)ρ for NABA-O2 and PNBA-O2 indicates the attractive part of Van der Waals (VdW) interactions. Both compounds showed intense spikes at -0.015 sign(λ2)ρ values, referring to the formation of weak interactions between the H atoms of the benzoic acid moieties and the O-O bridges (3D plots). However, the repulsive part of such VdW interactions, highlighted by the spikes at positive sign(λ2)ρ values (0.010-0.015) showed comparable intensity and steric effects could be observed (brown-red zone in 3D plot). The RGD analysis on PABA-O2 and ANBA-O2 are characterized again by intense spikes at sign(λ2)ρ values -0.010 ÷ -0.015 as previously observed, and an additional spike at -0.17 sign(λ2)ρ marking a stronger interaction between the H atoms of the benzoic acid moieties and the O-O bridges (3D plot). As reported for naphthalenes, the repulsive part showed intensity comparable to the attractive one, indicating again the presence of steric effects. Eventually, also the 2D RDG plot of DPAA-O2 showed intense spikes at -0.010 and +0.010 sign(λ_2)ρ due to vdW interactions.

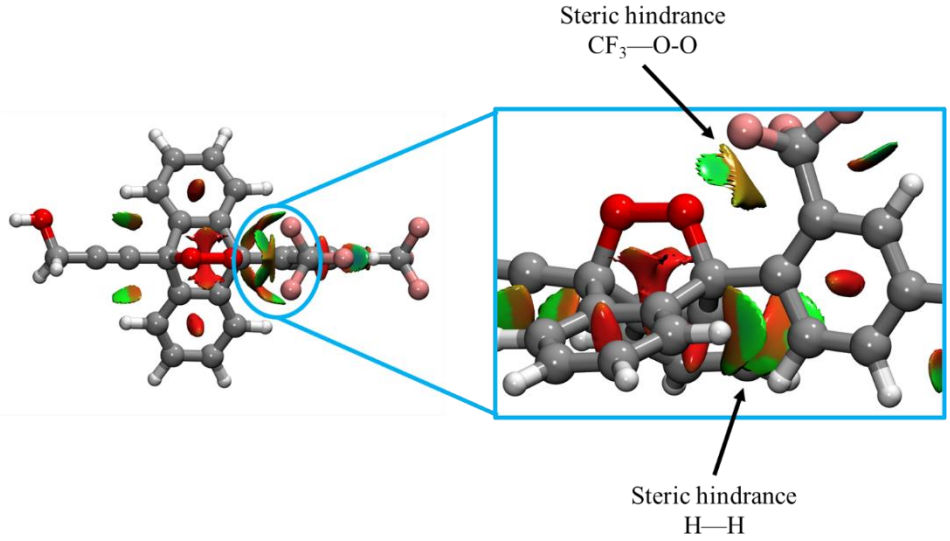

Figure S4: Reduced gradient density (RGD) isosurface for optimized structure 6 (see **Table S2**) at isovalue of 0.65: green zone attractive non covalent interaction, brown-red zone repulsive steric effect, red zone strong repulsion or strong steric effect in ring. Unfavourable steric effect between the CF_3 groups and the O-O bridge, as well as between the H atoms of the anthracene rings and the H atoms of tris-trifluoromethyl-benzene lead to a destabilization of the structure

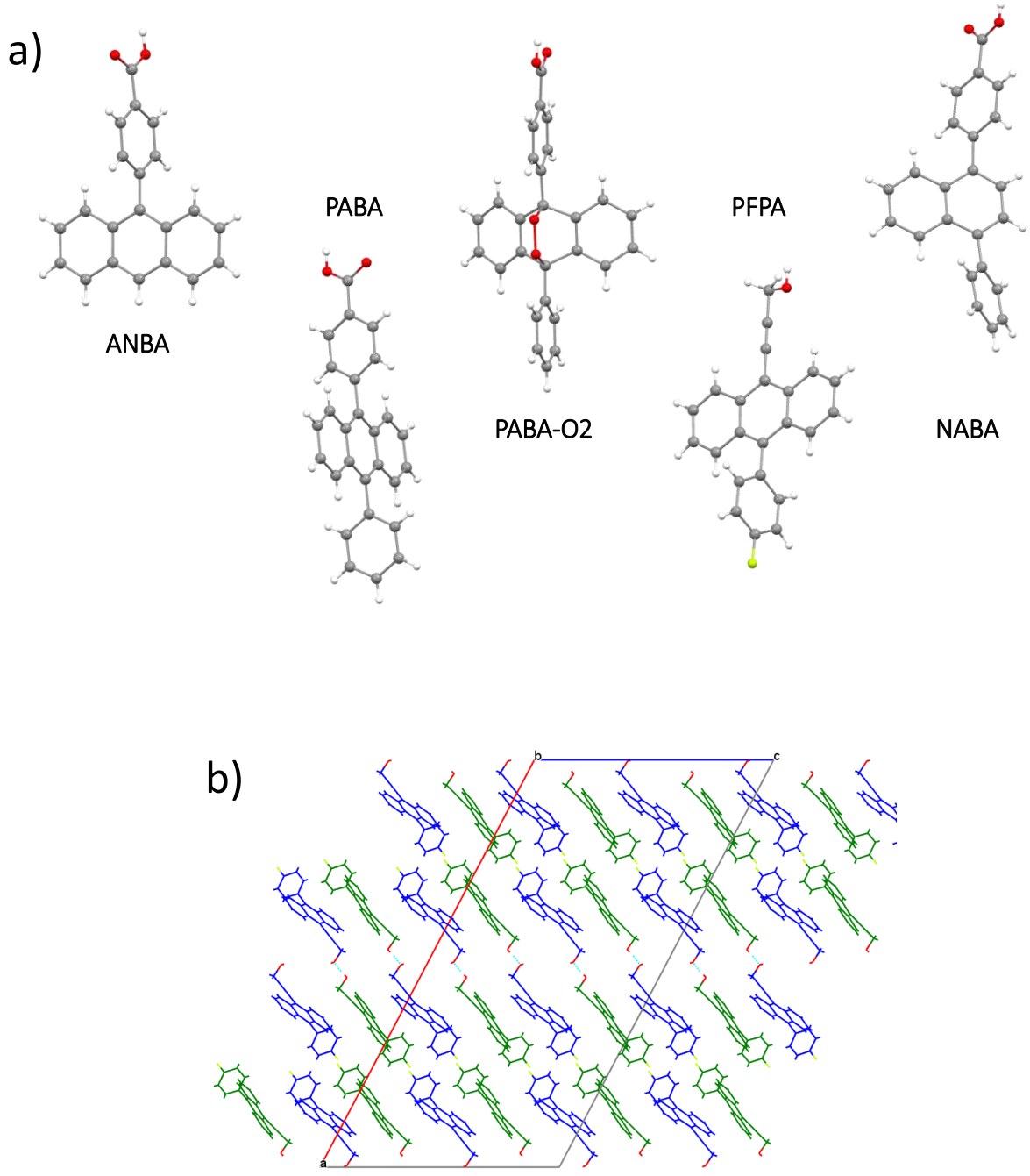

Figure S5: a) Crystal structures of **ANBA**, **PABA**, **PABA-O2**, **PFPA** and **PNBA**. b) View down the b axis of the crystal packing of **PFPA**. Light-blue dotted lines represent the O–H···O hydrogen bonds.

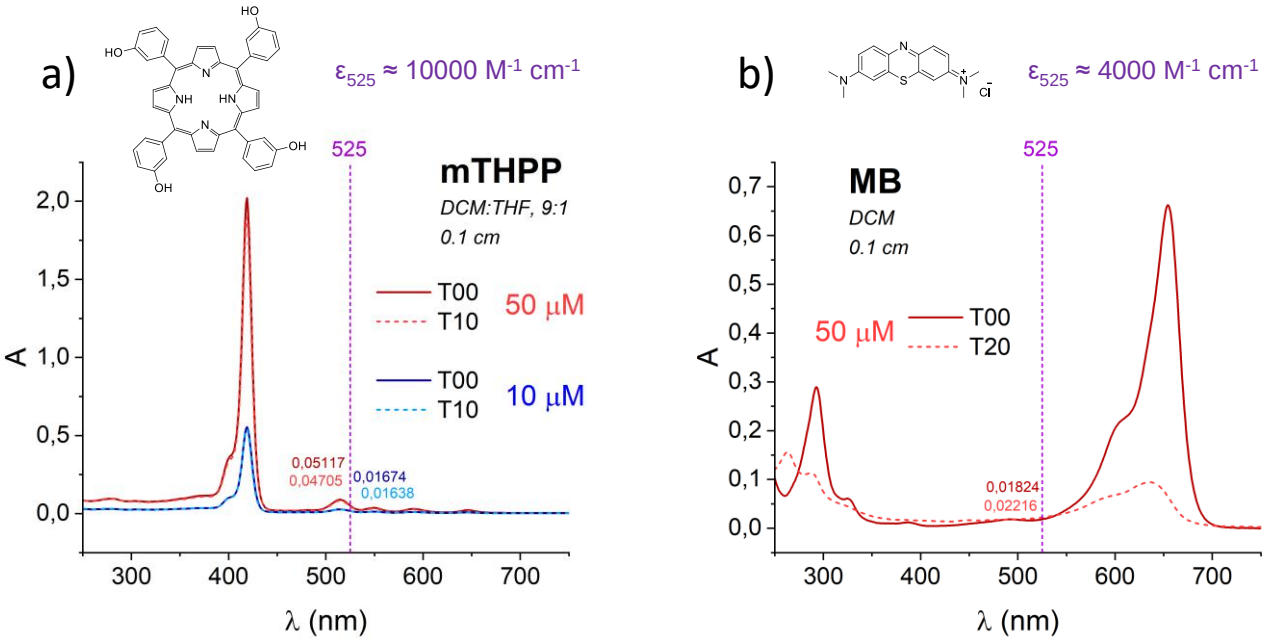

Figure S6: Stability of the tested PS, a) 5,10,15,20-tetrakis(3-hydroxyphenyl)-porphyrin (mTHPP) and b) methylene blue (MB) upon irradiation in flow at 525 nm, T_{set} = 25 °C.

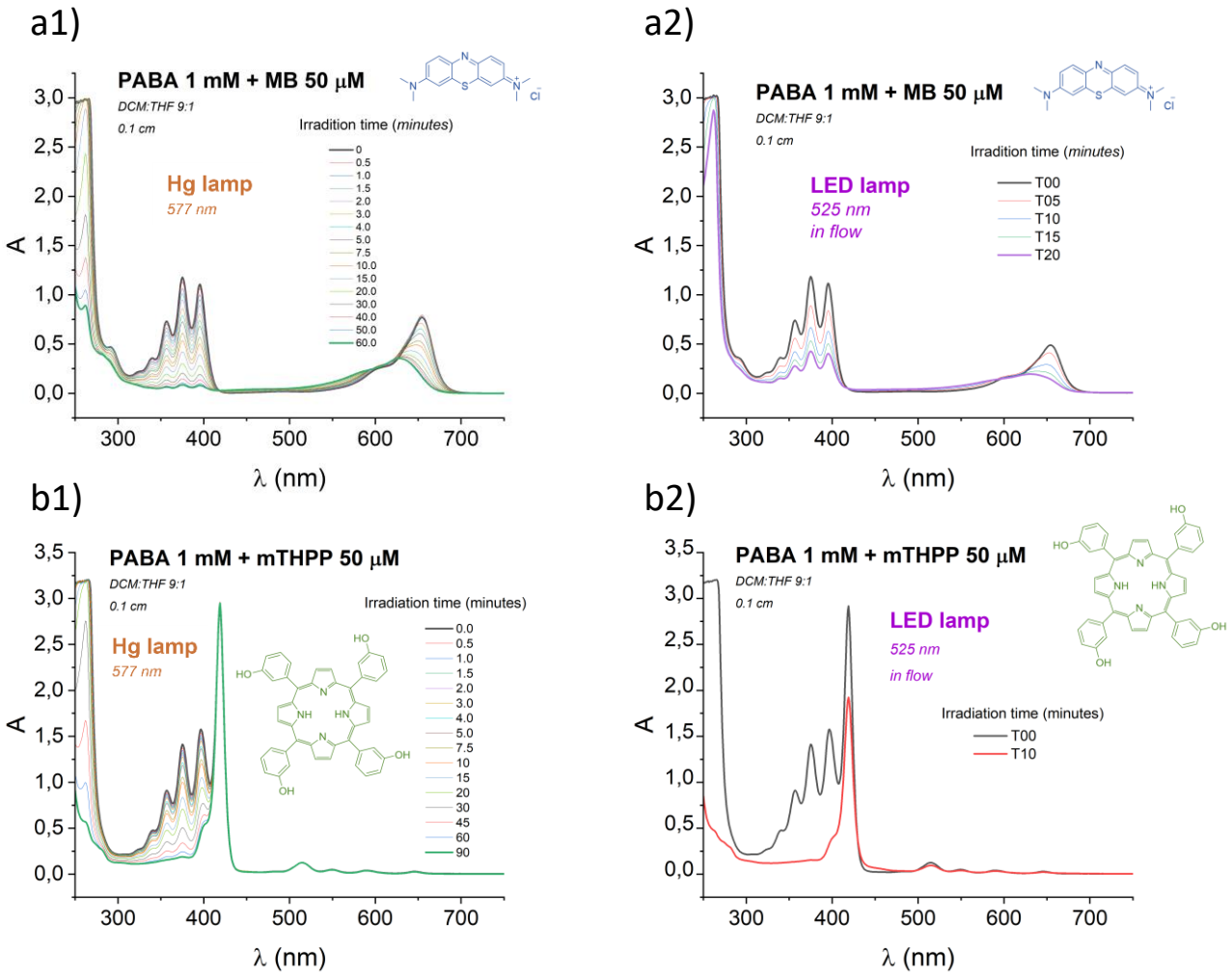

Figure S7: Comparison between two different irradiation setups: **1**) 100 W Hg-lamp equipped with a bandpass filter at 577 nm and **2**) the photochemical in flow reactor equipped with a 525 nm LED lamp, for the photosensitized conversion of PABA to PABA-O2 (1 mM) in the presence of the same amount (5% mol/mol, 50 µM) of the two tested PS, namely **a**) methylene blue (MB) and **b**) 5,10,15,20-tetrakis(3-hydroxyphenyl)-porphyrin (mTHPP). Reaction was performed in DCM : THF, 9 : 1 and UV-Vis spectra were acquired on Perkin-Elmer Lambda 950 in 0.1 cm cuvettes.

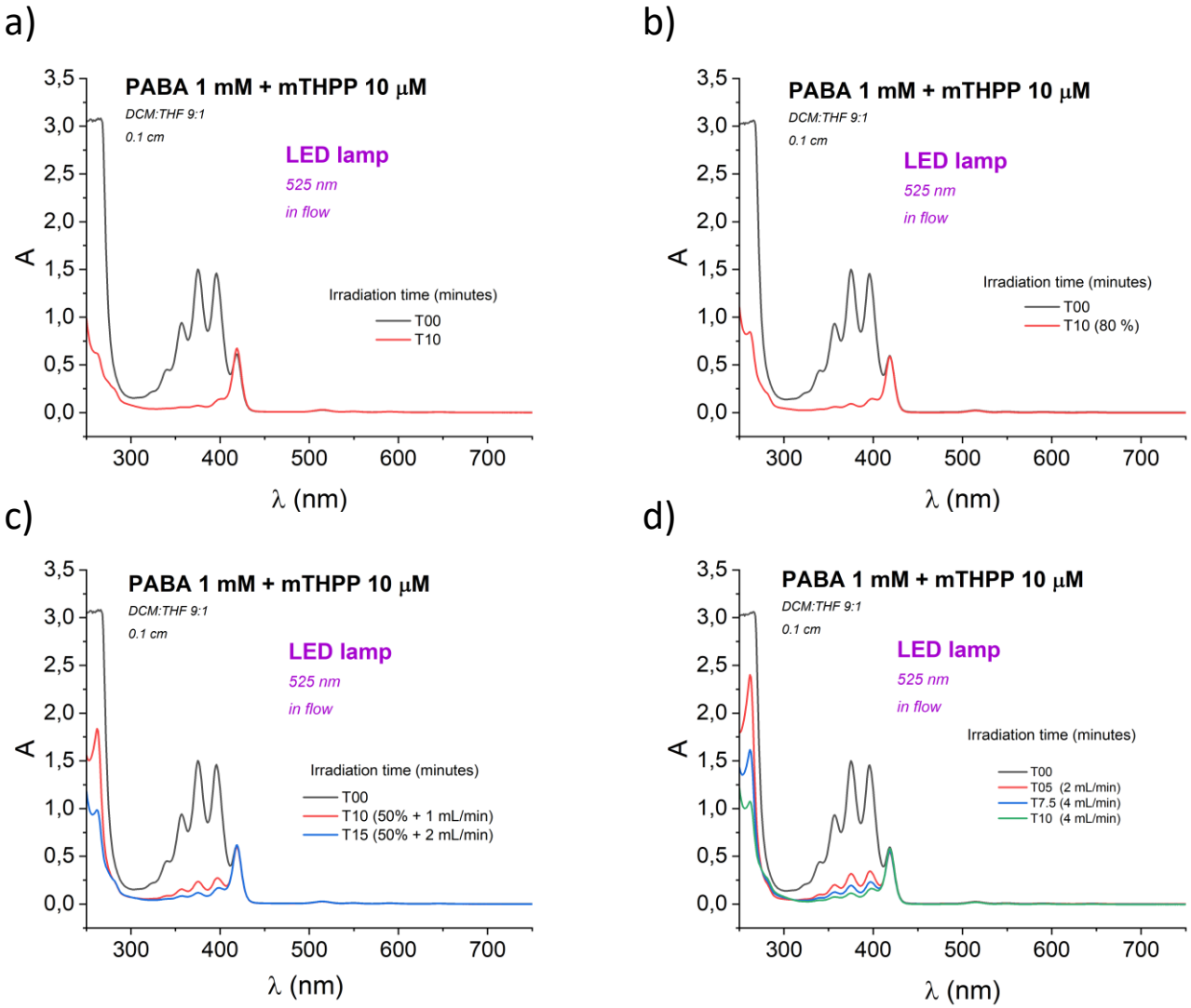

Figure S8: Different conditions tested for the photochemical conversion of PABA (1 mM) to PABA-O2 in the presence of mTHPP (10 µM, 1% mol/mol) using the LED lamp at 525 nm at a) 100 % of intensity, b) 80 % of intensity, c) 50 % of intensity and d) 100 % of intensity at different flow rates: 2 or 4 mL min^{-1}. The use of a LED lamp emitting at 425 nm was not pursued since it resulted in full quenching of the mTHPP and MB upon irradiation at T_{set} = 25°C (results not shown).

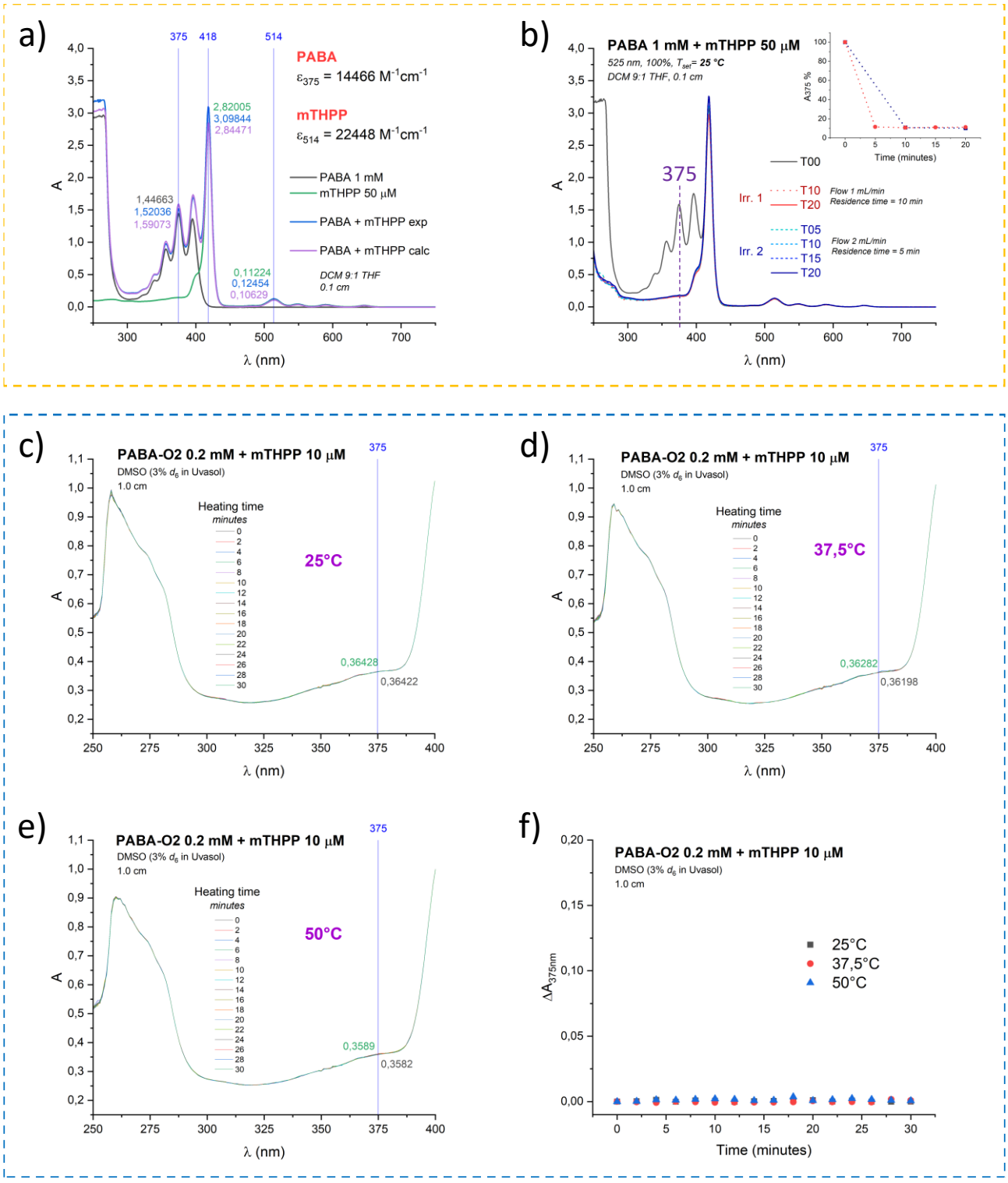

Figure S9: Yellow box: absorption spectra monitoring a) the profiles of PABA, mTHPP and their calculated and experimental sums and b) the formation of PABA-O2 (inset A% at 375 nm, Lambda 950, 0.1 cm cuvette); Blue box: absorption spectra monitoring the release of O_2 from PABA-O2 at 375 nm at c) 25 °C, d) 37.5 °C and e) 50 °C; f) kinetic profile of the O_2 release from PABA-O2 at different temperatures (Agilent CARY 100, 1.0 cm cuvette).

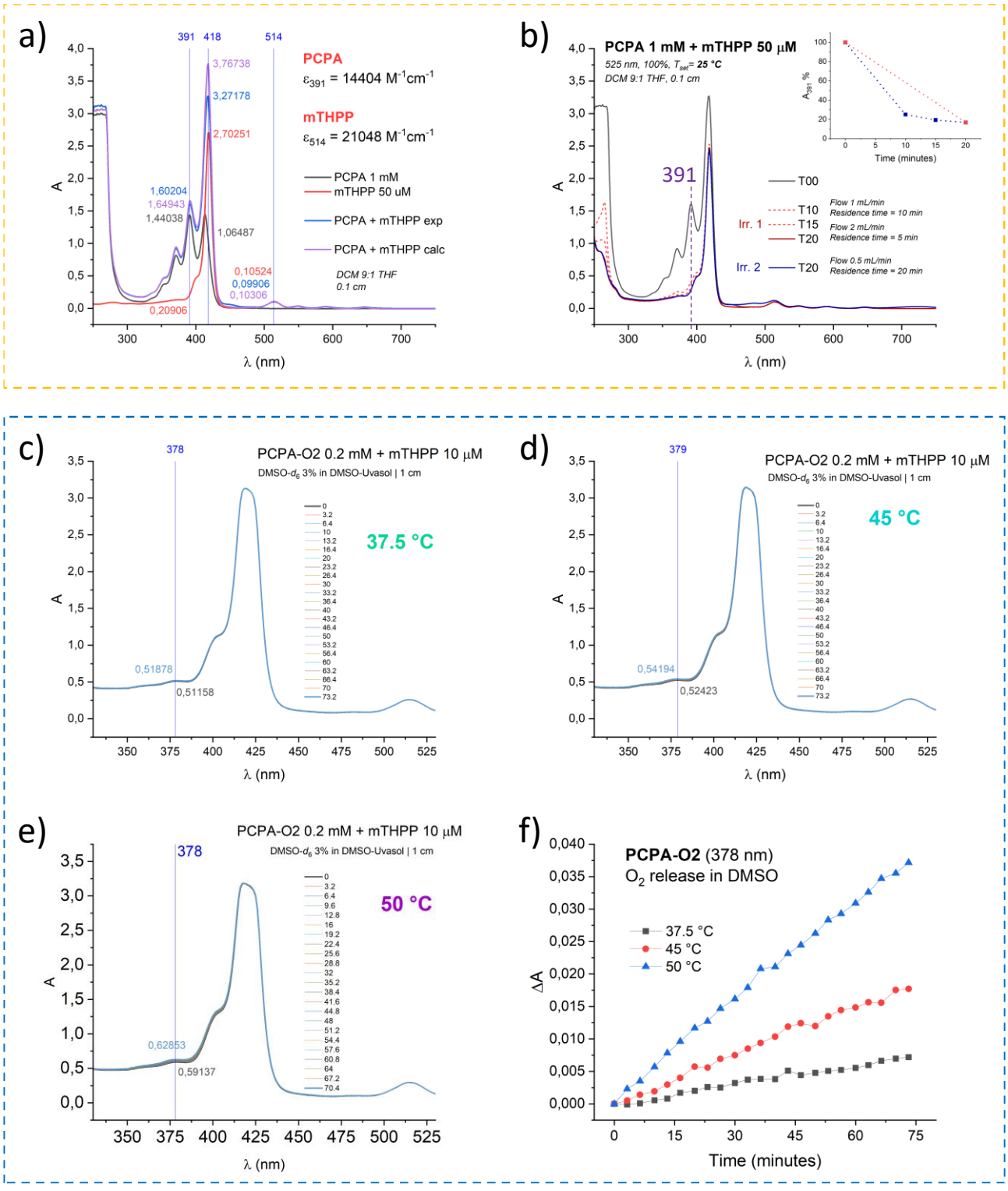

Figure S10: Yellow box: absorption spectra monitoring a) the profiles of PCPA, mTHPP and their calculated and experimental sums and b) the formation of PCPA-O2 (inset A% at 391 nm, Lambda 950, 0.1 cm cuvette); Blue box: absorption spectra monitoring the release of O_2 from PCPA-O2 at c) 37.5 °C, d) 45 °C and e) 50 °C; f) kinetic profile of the O_2 release from PCPA-O2 (at 378 nm) at different temperatures (Agilent CARY 100, 1.0 cm cuvette).

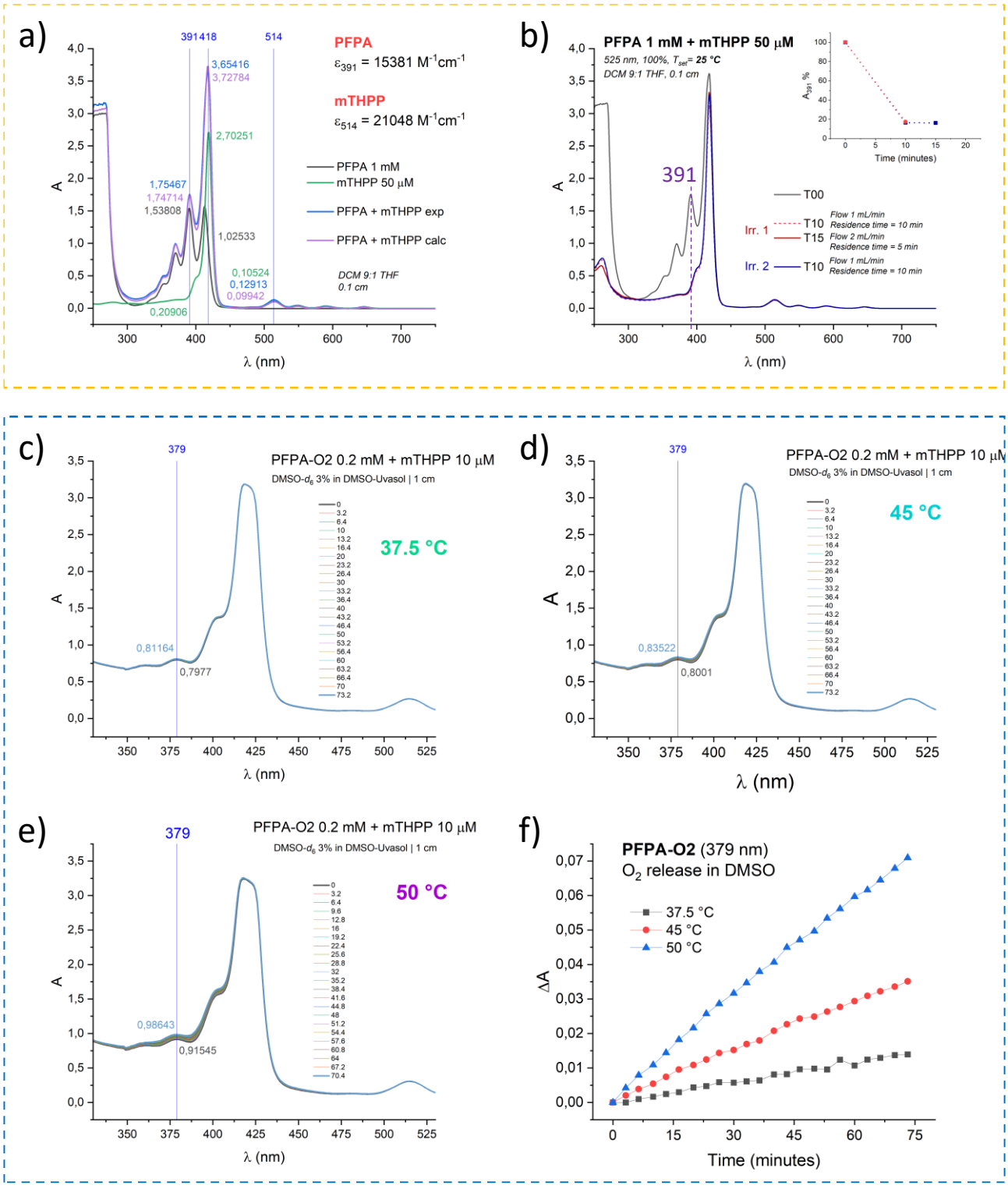

Figure S11: Yellow box: absorption spectra monitoring a) the profiles of PFPA, mTHPP and their calculated and experimental sums and b) the formation of PFPA-O2 (inset A% at 391 nm, Lambda 950, 0.1 cm cuvette); Blue box: absorption spectra monitoring the release of O_2 from PFPA-O2 at c) 37.5 °C, d) 45 °C and e) 50 °C; f) kinetic profile of the O_2 release from PFPA-O2 (at 379 nm) at different temperatures (Agilent CARY 100, 1.0 cm cuvette).

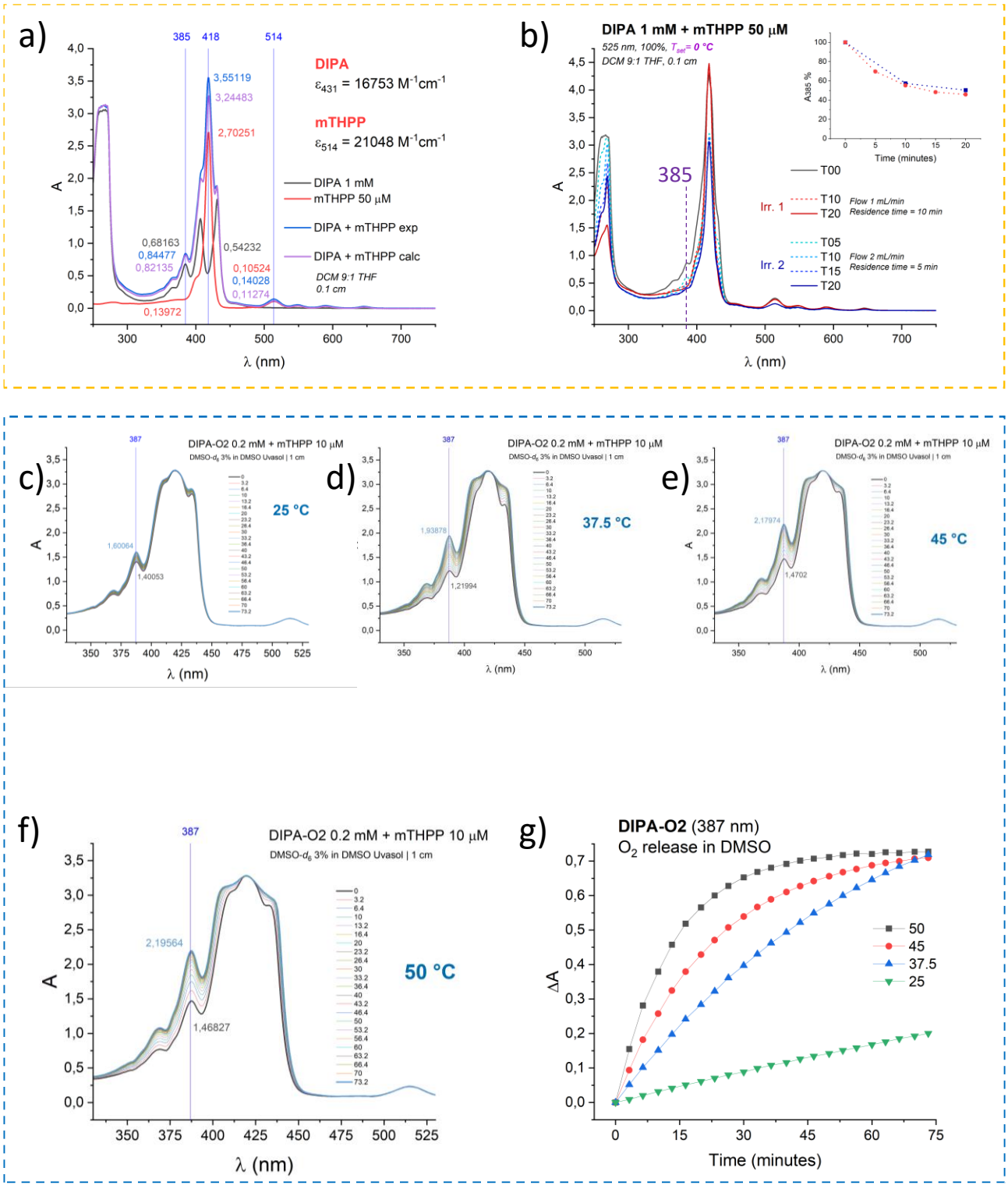

Figure S12: Yellow box: absorption spectra monitoring a) the profiles of DIPA, mTHPP and their calculated and experimental sums and b) the formation of DIPA-O2 (inset A% at 385 nm, Lambda 950, 0.1 cm cuvette); Blue box: absorption spectra monitoring the release of O_2 from DIPA-O2 at c) 25 °C, d) 37.5 °C and e) 45 °C and f) 50 °C; g) kinetic profile of the O_2 release from DIPA-O2 (at 387 nm) at different temperatures (Agilent CARY 100, 1.0 cm cuvette).

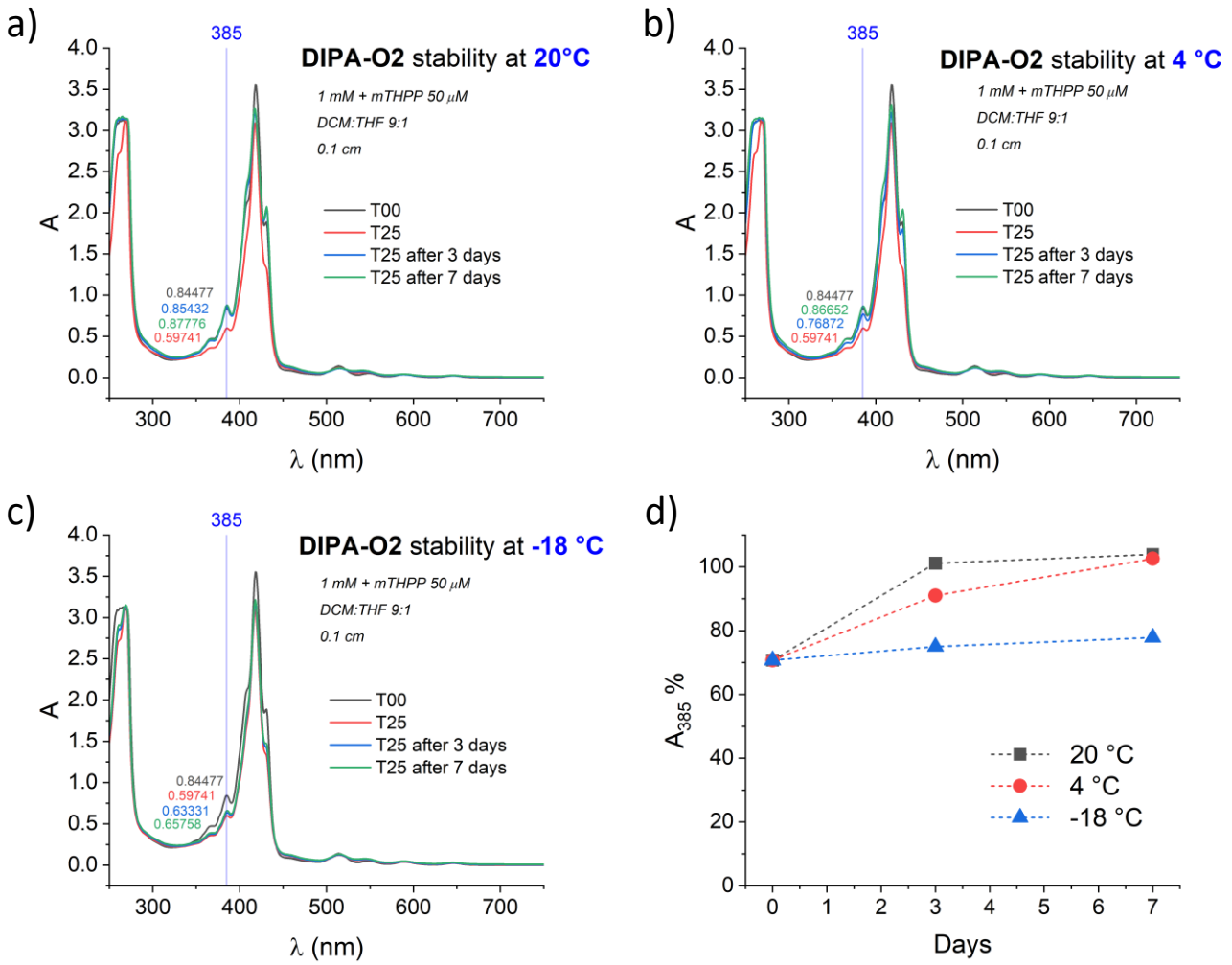

Figure S13: Stability of DIPA-O2 (1 mM) in DCM:THF, 9:1 in the presence of mTHPP (50 µM) after storage at a) 20 °C, b) 4 °C and c) -18 °C; d) Variation of the maximum absorption peak at 385 nm as a function of time after storage at three different temperatures.

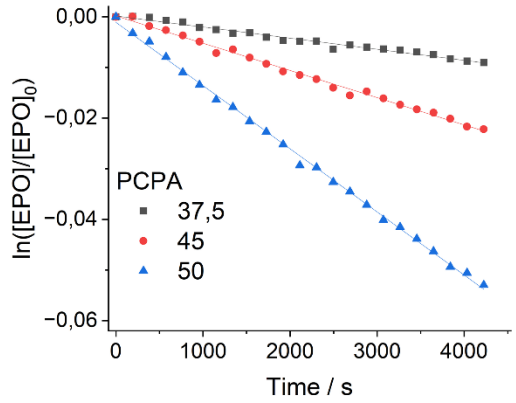

Equation	y = a + b*x		
Plot	37.5	45	50
Weight		No Weighting	
Intercept	2,49411E-4 ± 2,32739E-4	2,59474E-4 ± 3,03046E-4	-0,00128 ± 3,28263E-4
Slope	-3,00769E-6 ± 9,43682E-8	-7,39869E-6 ± 1,22875E-7	-1,54622E-5 ± 1,331E-7
Residual Sum of Squares	6,97676E-6	1,18286E-5	1,3879E-5
Pearson's r	-0,98982	-0,99712	-0,99922
R-Square (COD)	0,97975	0,99424	0,99845
Adj. R-Square	0,97878	0,99397	0,99837

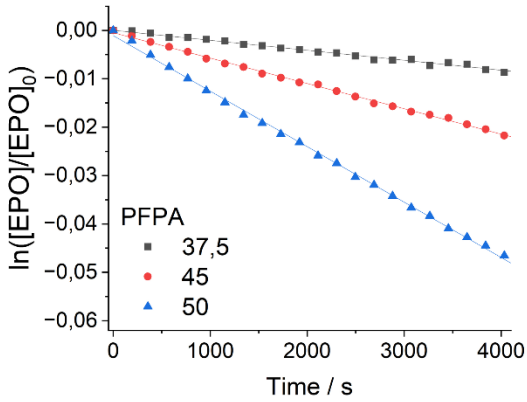

Equation	y = a + b*x		
Plot	37.5	45	50
Weight		No Weighting	
Intercept	2,26761E-5 ± 1,91304E-4	-7,0924E-4 ± 1,7696E-4	-0,00141 ± 3,02768E-4
Slope	-3,1341E-6 ± 7,75676E-8	-7,98986E-6 ± 7,17518E-8	-1,62171E-5 ± 1,22763E-7
Residual Sum of Squares	4,71372E-6	4,03337E-6	1,18069E-5
Pearson's r	-0,99363	-0,99915	-0,9994
R-Square (COD)	0,9873	0,99831	0,9988
Adj. R-Square	0,9867	0,99823	0,99874

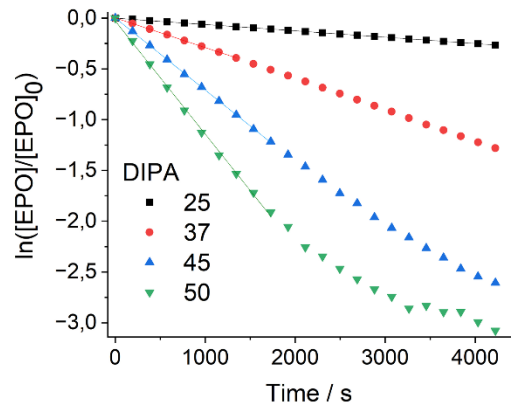

Equation	y = a + b*x
Plot	25
Weight	No Weighting
Intercept	-9,12193E-5 ± 2,8904E-4
Slope	-6,27063E-5 ± 1,17197E-7
Residual Sum of Squares	1,07605E-5
Pearson's r	-0,99996
R-Square (COD)	0,99993
Adj. R-Square	0,99992

Equation	y = a + b*x
Plot	37.5
Weight	No Weighting
Intercept	0,00296 ± 0,00127
Slope	-2,93188E-4 ± 1,58657E-6
Residual Sum of Squares	2,33843E-5
Pearson's r	-0,99991
R-Square (COD)	0,99982
Adj. R-Square	0,9998

Equation	y = a + b*x
Plot	45
Weight	No Weighting
Intercept	5,93078E-4 ± 0,00298
Slope	-7,09088E-4 ± 2,90942E-6
Residual Sum of Squares	2,05949E-4
Pearson's r	-0,99993
R-Square (COD)	0,99987
Adj. R-Square	0,99985

Equation	y = a + b*x
Plot	50
Weight	No Weighting
Intercept	-0,02929 ± 0,01689
Slope	-0,00111 ± 1,6482E-5
Residual Sum of Squares	0,00661
Pearson's r	-0,99912
R-Square (COD)	0,99825
Adj. R-Square	0,99803

Figure S14: Summary of the kinetic analysis obtained by fitting of the UV-Vis data monitoring the release of O_2 from different EPOs at 25, 37.5, 45 and 50 °C (0.2 mM in 3% DMSO-d_6 in DMSO Uvasol, 1 cm cuvettes).

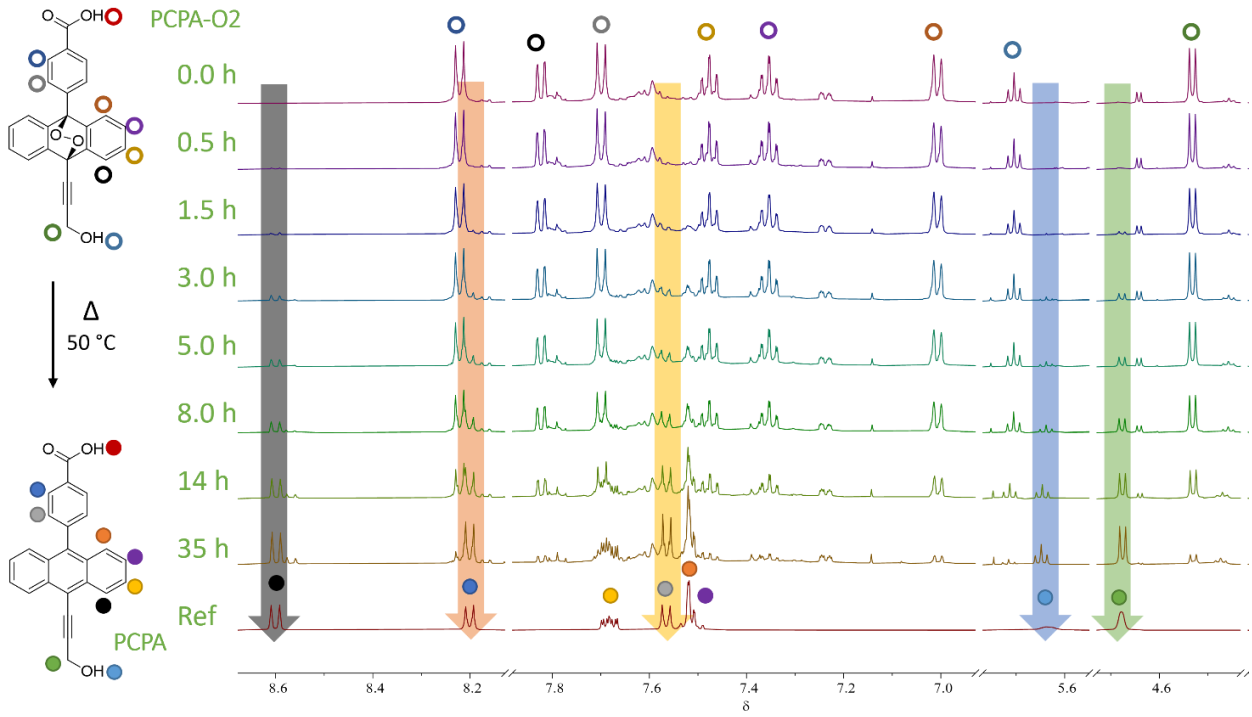

Figure S15: ^{1}H NMR spectra (500 MHz, 298 K, 32 scans, relaxation delay = 1 s) monitoring the conversion of PCPA-O2 (6 mM in DMSO-d_6) to PCPA by heating at 50 °C. Arrows indicate the growing peaks of PCPA.

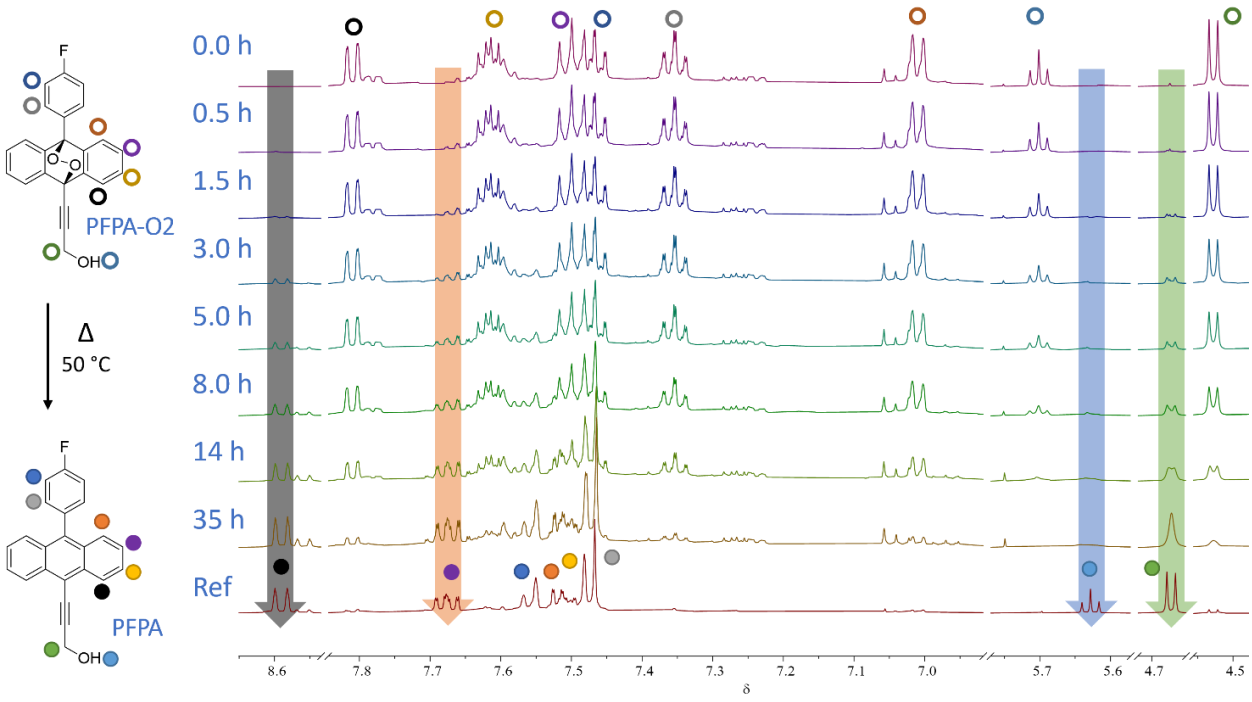

Figure S16: ^{1}H NMR spectra (500 MHz, 298 K, 32 scans, relaxation delay = 1 s) monitoring the conversion of PFPA-O2 (6 mM in DMSO-d_6) to PFPA by heating at 50 °C. Arrows indicate the growing peaks of PFPA.

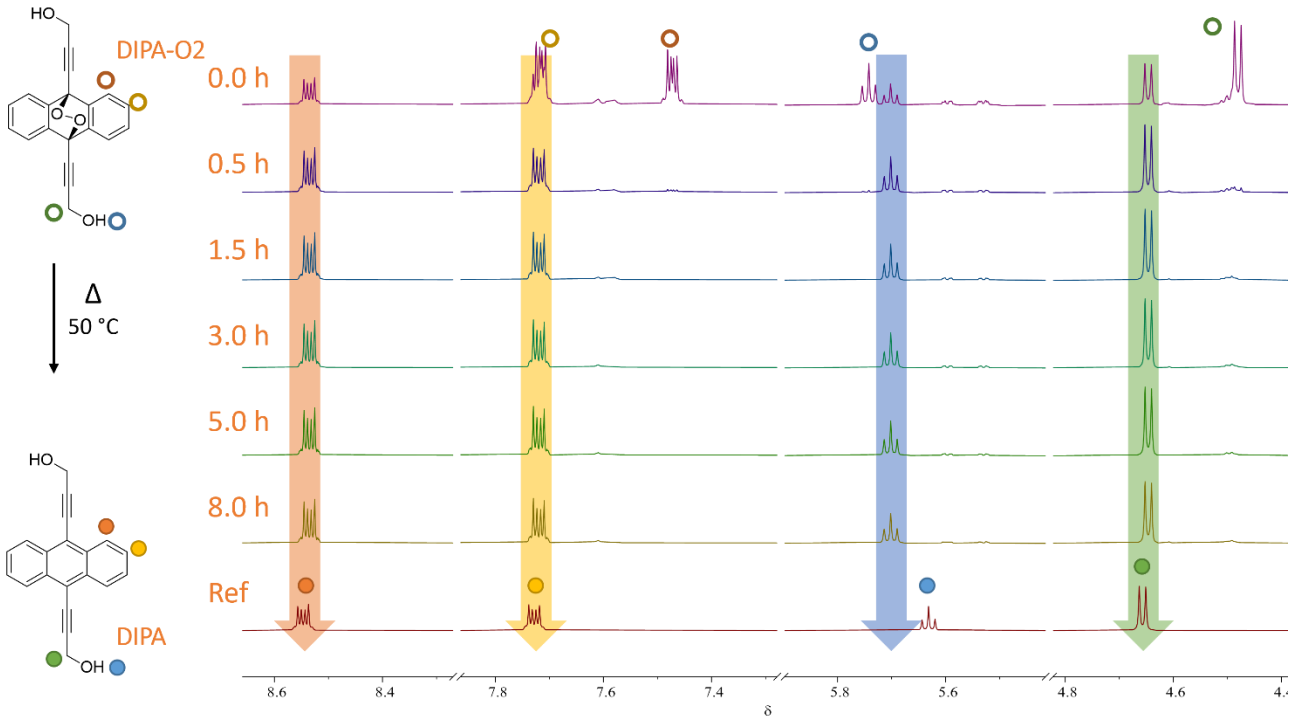

Figure S17: ^{1}H NMR spectra (500 MHz, 298 K, 32 scans, relaxation delay = 1 s) monitoring the conversion of DIPA-O2 (6 mM in DMSO-d_6) to DIPA by heating at 40 °C. Arrows indicate the growing peaks of DIPA.

3. Synthetic procedures

2.1 General

The synthesis of **PABA** and 4-methoxycarbonylphenylboronic acid (mCPBA) were achieved following published procedures.[26] For all synthetic steps, the glassware was dried overnight in an oven set at 100 °C. When needed, an aqueous solution of Cs_2CO_3 (2 M) was prepared fresh before each use. The solvent THF was distilled and collected over molecular sieves before each use. The assignment of ^1H and ^{13}C NMR spectra was achieved after analysis of the two-dimensional ^1H-^1H COSY, ^1H-^{13}C HSQC, ^1H-^{13}C HMBC and 2D ROESY NMR experiments.

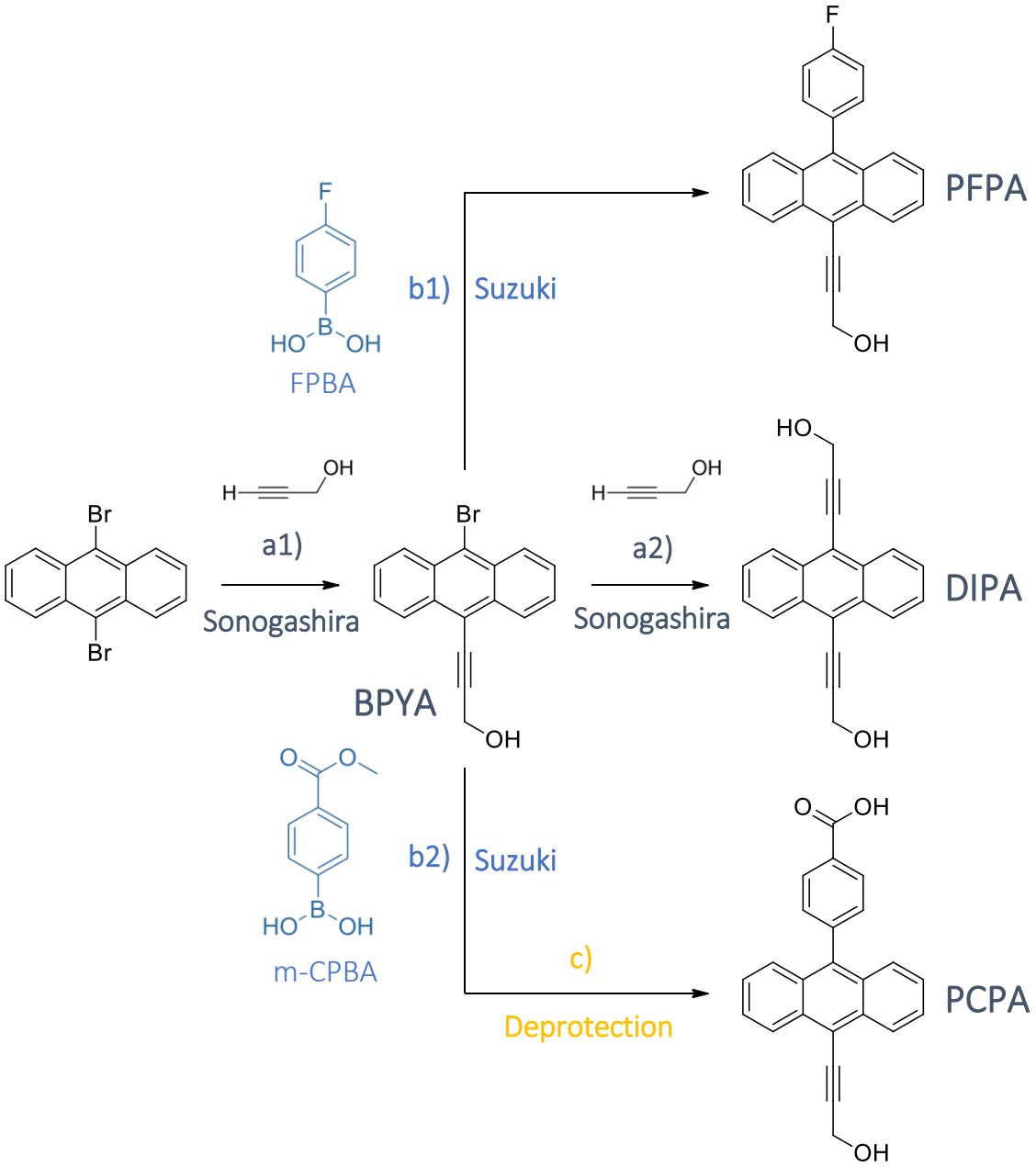

Scheme S1: synthetic steps for the formation of **DIPA**, **PCPA** and **PFPA**.

2.2 Sonogashira couplings (a)[27,28]

9-bromo-10-prop-2-yn-1-ol-anthracene (BPYA) and 9,10-diprop-2-yn-1-ol-anthracene (DIPA)

9,10-Dibromoanthracene (DBA, 0.503 g, 1.5 mmol), di*iso*propylamine (8 mL, 57 mmol), copper iodide (CuI, 0.178 g, 0.9 mmol) and $Pd(PPh_3)_2Cl_2$ (0.108 g, 0.15 mmol) were dissolved in distilled THF (15 mL) and placed in a round-bottom falsk. The solution was kept under N_2 atmosphere and then immersed in an oil bath with T_{set} = 85 °C. Once the mix started refluxing, propargyl alcohol (0.2 mL, 3.4 mmol) was added in 10 aliquots over a period of 90 minutes. The clear yellow solution turned black and it was left to stir and reflux under N_2 atmosphere for further 16 h. After TLC monitoring (*n*-hexane : AcOEt 4 : 1, Rf_{DBA} = 0.9, Rf_{BPYA} = 0.5, Rf_{DIPA} = 0.3), a second fraction of reactants (di*iso*propylamine: 8 mL, 57 mmol, CuI: 0.180 g, 0.9 mmol, $Pd(PPh_3)_2Cl_2$: 0.107 g, 0.15 mmol) was added to the mixture which was left to stir in the same conditions for further 5 h. After TLC monitoring, a final fraction of reactants (di*iso*propylamine: 8 mL, 57 mmol, CuI: 0.180 g, 0.9 mmol, $Pd(PPh_3)_2Cl_2$: 0.103 g, 0.15 mmol) was added to the mixture which was left to stir again in the same conditions (reflux, N_2 atmosphere) for further 18 h. After TLC check, the reaction was stopped. The mixture was cooled to r.t. and the solvent was evaporated to dryness under *vacuum*. The solid, dark residue was dissolved in ethyl acetate (AcOEt, 70 mL) and washed with brine (70 mL). The aqueous layer was washed with AcOEt (5 x 30 mL) and all the organic fractions were collected and dried over anhydrous Na_2SO_4 for 1 h. The yellow solution was filtered on paper before removal of the solvent under *vacuum*. The crude residue (1.4 g) was adsorbed on SiO_2 (4.5 g) and purified by column chromatography on SiO_2 (85 g), eluting with a gradient of solvents from *n*-hexane to *n*-hexane : AcOEt 6 : 4. The final products were obtained after removal of the solvent under *vacuum*.

9-bromo-10-prop-2-yn-1-ol-anthracene (**BPYA**): 0.160 g, 0.51 mmol → 27% yield, yellow powder. **^{1}H NMR (500 MHz, DMSO-d_6)** δ 8.59 (d, *J* = 8.1 Hz, 2H), 8.50 (d, *J* = 8.5 Hz, 2H), 7.79-7.75 (m, 4H), 5.68-5.64 (broad, 1H), 4.65-4.64 (broad, 2H). **^{13}C NMR (125 MHz, DMSO-d_6)** δ 132.3, 129.5, 128.4, 127.6, 127.6, 126.9, 122.9, 117.7, 103.2, 79.4, 50.0.

9,10-diprop-2-yn-1-ol-anthracene (**DIPA**): The fractions containing the product were dissolved in the minimum amount of THF (1 mL) and then copious an excess of DCM was added (20 mL). The solution was allowed to cool at 0°C and the ellow precipitate was filtered on Buchner yielding 0.118 g of **DIPA** (0.41 mmol, 27 % yield). **^{1}H NMR (500 MHz, DMSO-d_6)** δ 8.55 (dd, *J* = 6.6, 3.3 Hz, 4H), 7.73 (dd, *J* = 6.7, 3.2 Hz, 4H), 5.64 (t, *J* = 6.0 Hz, 2H), 4.66 (d, *J* = 6.0 Hz, 4H).**^{13}C NMR (125 MHz, DMSO-d_6)** δ 131.3, 127.4, 126.7, 117.5, 103.4, 79.7, 50.0. **ESI-MS$^+$**: m/z calc: 286; found: 309 $[DIPA+Na]^+$.

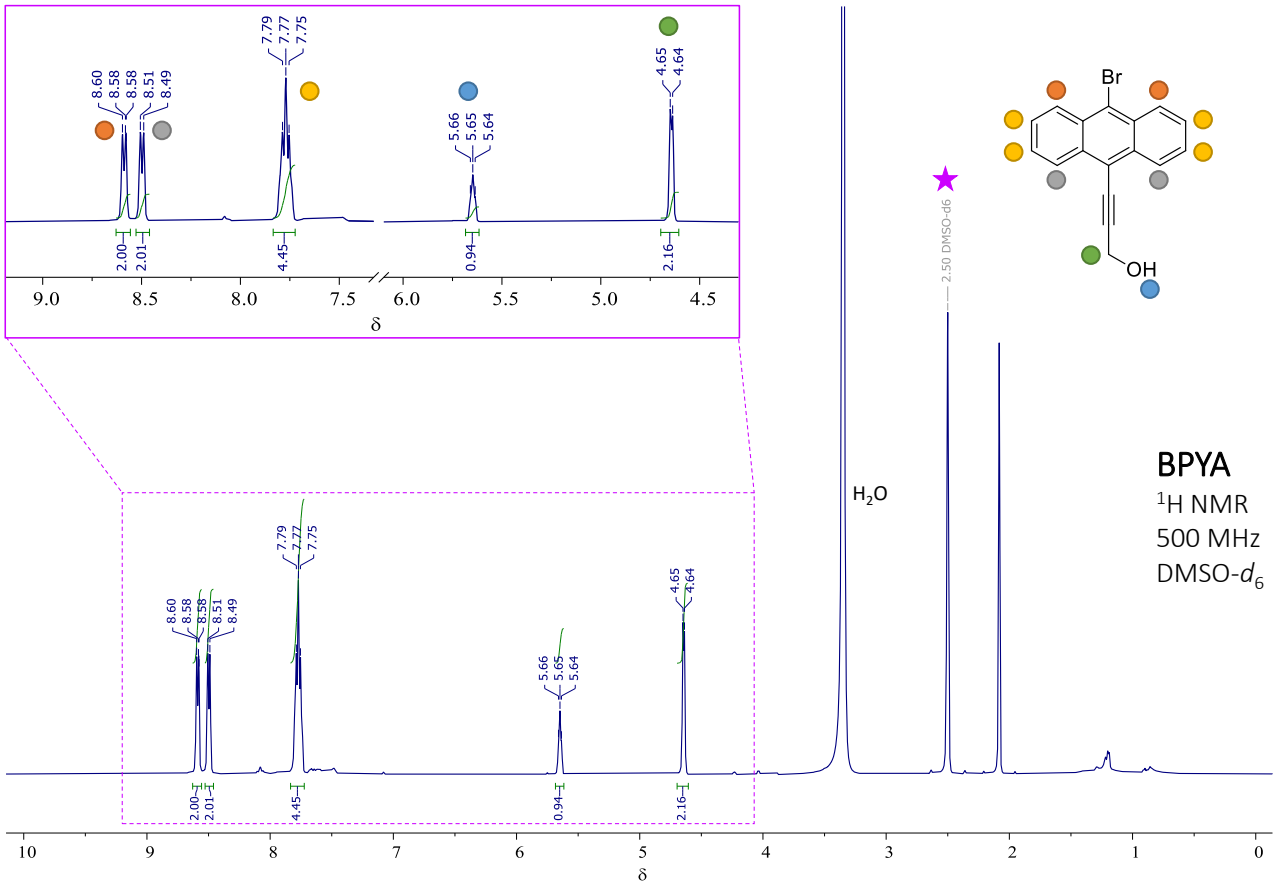
8.60
8.58
8.58
8.51
8.49
7.79
7.77
7.75
5.66
5.65
5.64
4.65
4.64
2.00
2.01
4.45
0.94
2.16
δ
H2O
2.50 DMSO-d6
Br
OH
BPYA
1H NMR
500 MHz
DMSO-d6

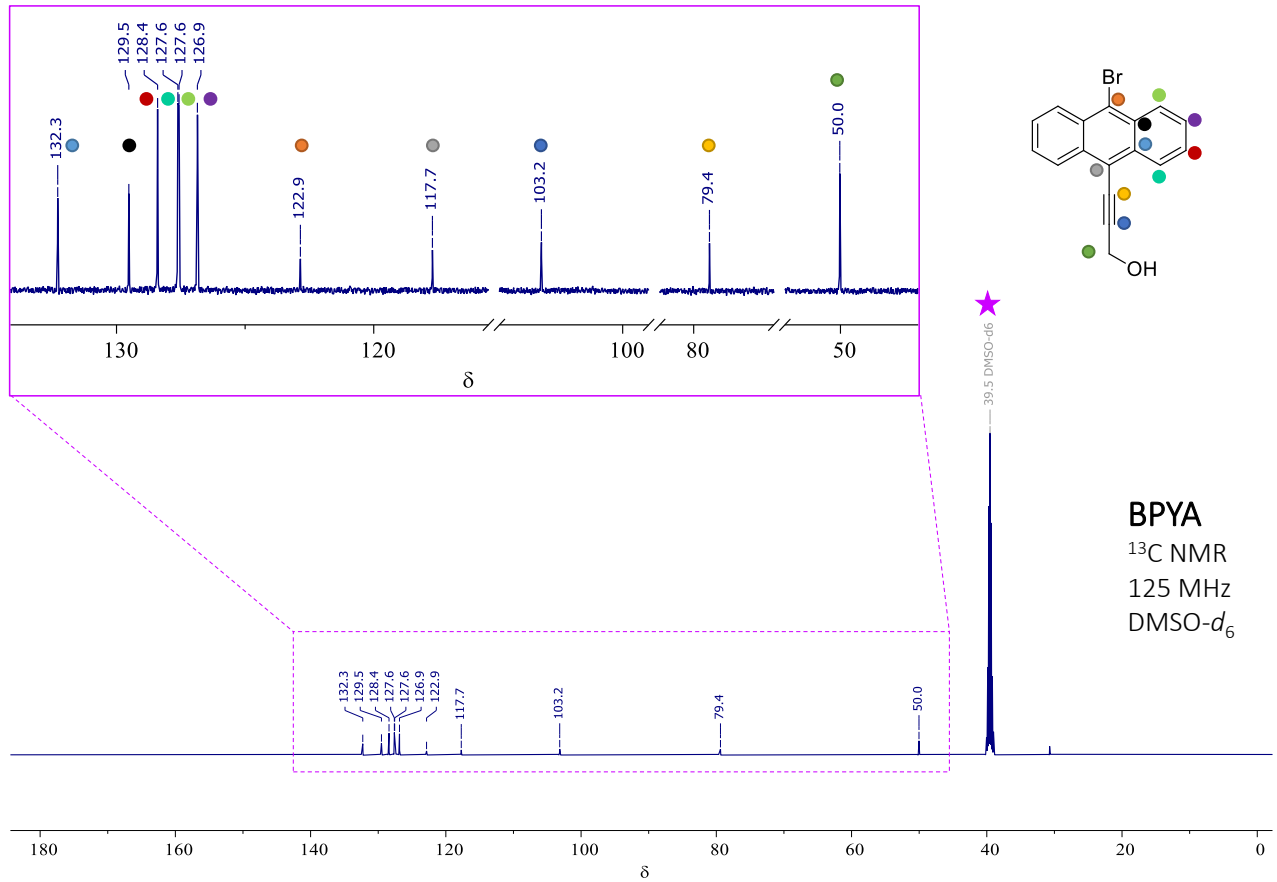
132.3
129.5
128.4
127.6
127.6
126.9
122.9
117.7
103.2
79.4
50.0
δ
39.5 DMSO-d6
Br
OH
BPYA
13C NMR
125 MHz
DMSO-d6

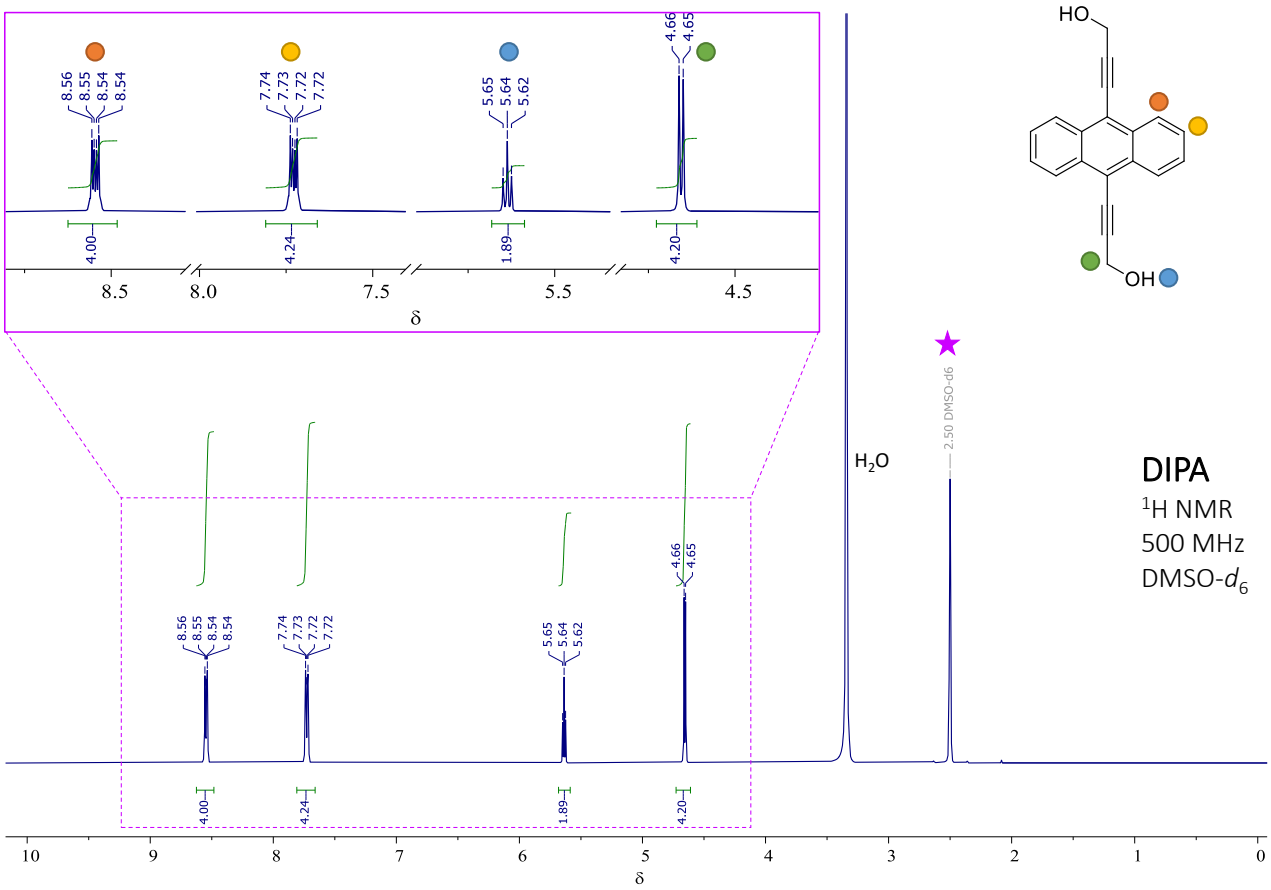
HO
OH
8.56
8.55
8.54
8.54
7.74
7.73
7.72
7.72
5.65
5.64
5.62
4.66
4.65
4.00
4.24
1.89
4.20
8.5
8.0
7.5
5.5
4.5
δ
H2O
2.50 DMSO-d6
DIPA
1H NMR
500 MHz
DMSO-d6
10
9
8
7
6
5
4
3
2
1
0

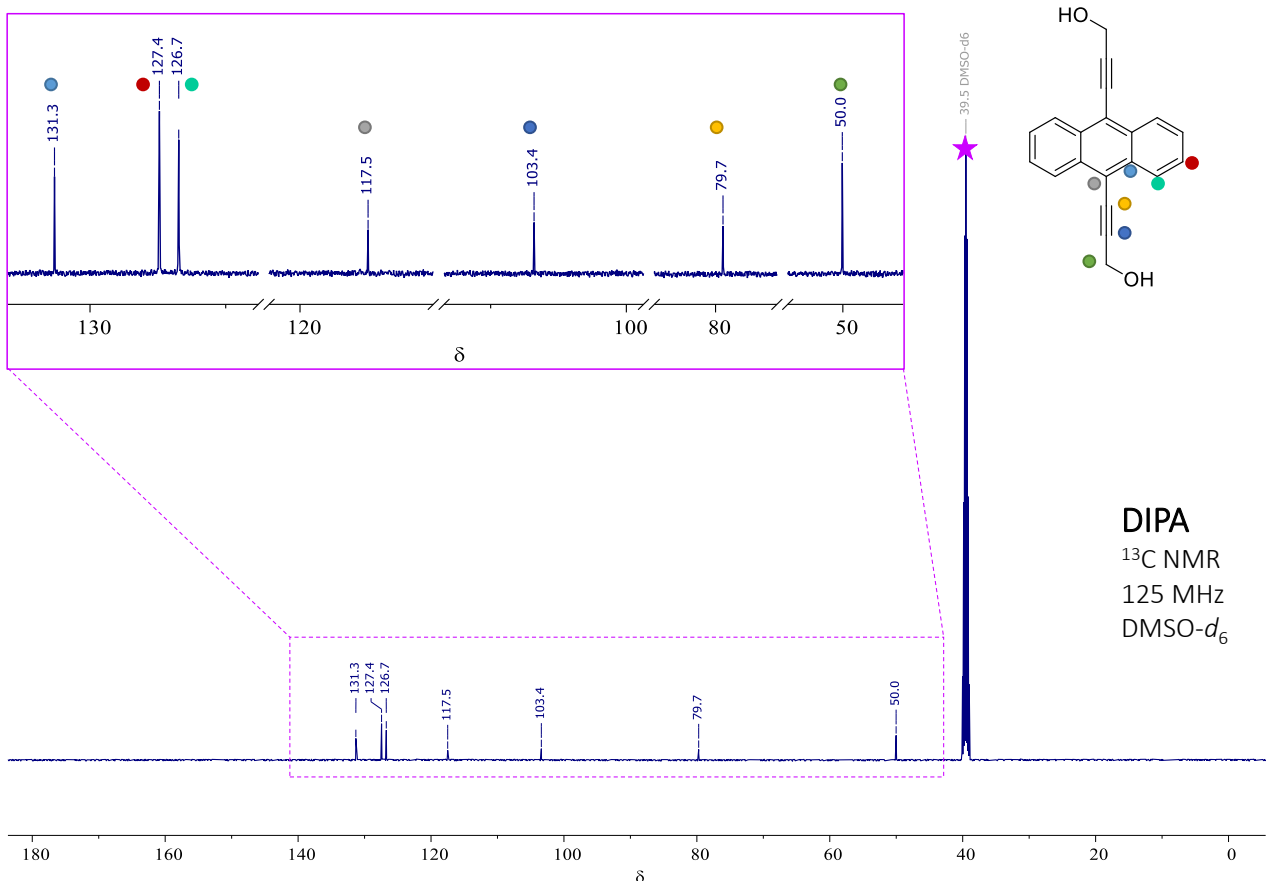
HO
OH
131.3
127.4
126.7
117.5
103.4
79.7
50.0
39.5 DMSO-d6
130
120
100
80
50
δ
DIPA
13C NMR
125 MHz
DMSO-d6
180
160
140
120
100
80
60
40
20
0

2.3 Suzuki couplings (b)[26]

9-(4-fluorophenyl)-10-prop-2-yn-1-ol-anthracene (PFPA)

9-bromo-10-prop-2-yn-1-ol-anthracene (**BPYA**, 0.080 g, 0.26 mmol) was dissolved in freshly distilled THF (3 mL) under vigorous stirring (500 rpm), placed in a round-bottom flask, kept under N_2 atmosphere and heated in an oil bath (T_{set} = 85 °C). (4-Fluorophenyl)boronic acid (FPBA, 0.028 g, 0.20 mmol), aqueous Cs_2CO_3 (2 M, 0.2 mL, 0.4 mmol) and $Pd(PPh_3)_4$ (0.0134 g, 0.012 mmol) were added together when T_{int} = 40 °C. The mixture resulted in a homogeneous, clear, intense yellow solution. As soon as the reaction started refluxing, it was left to stir for 5 h. After TLC monitoring (*n*-hexane : AcOEt 4 : 1, Rf_{BPYA} = 0.5, Rf_{PFPA} = 0.4) a second portion of reactants was added to the reaction mix (FPBA: 0.029 g, 0.20 mmol, Cs_2CO_3 2 M: 0.2 mL, 0.4 mmol, $Pd(PPh_3)_4$: 0.0144 g, 0.012 mmol) and the obtained solution was diluted with THF (3 mL) and then refluxed overnight for further 16 h.

After TLC monitoring the reaction was stopped. The mixture was cooled to r.t. and the solvent was evaporated to dryness under *vacuum*. The residue was dissolved in ethyl acetate (AcOEt, 10 mL) and washed with brine (10 mL). The aqueous layer was washed with AcOEt (3 x 20 mL) and all the organic fractions were collected and dried over anhydrous Na_2SO_4 for 0.5 h. The solution was filtered on paper before removal of the solvent under *vacuum*. The crude residue (0.15 g) was adsorbed on SiO_2 (1.9 g) and purified by column chromatography on SiO_2 (20 g), eluting with a gradient of solvents from *n*-hexane to *n*-hexane : AcOEt 4 : 1. The final product was obtained after removal of the solvent under *vacuum* (**PFPA**, 0.0393 g, 0.12 mmol, 46 % yield).

^{1}H NMR (500 MHz, $CDCl_3$) δ 8.62 (d, *J* = 8.8 Hz, 2H), 7.63 (d, *J* = 8.8 Hz, 2H), 7.60-7.54 (m, 2H), 7.43-7.35 (m, 4H), 7.30-7.27 (m, 2H), 4.87 (d, *J* = 6.1 Hz, 2H), 1.94 (t, *J* = 6.2 Hz, 1H). **^{13}C NMR (125 MHz, $CDCl_3$)** δ 163.6, 161.7, 137.6, 134.4, 134.3, 132. 9, 132.8, 132.6, 130.1, 127.2, 126.9, 126.6, 125.9, 117.0, 115.7, 115.6, 98.9, 82.7, 52.4.

ESI-MS$^-$: m/z calc: 326; found: 361 $[PFPA+Cl]^-$.

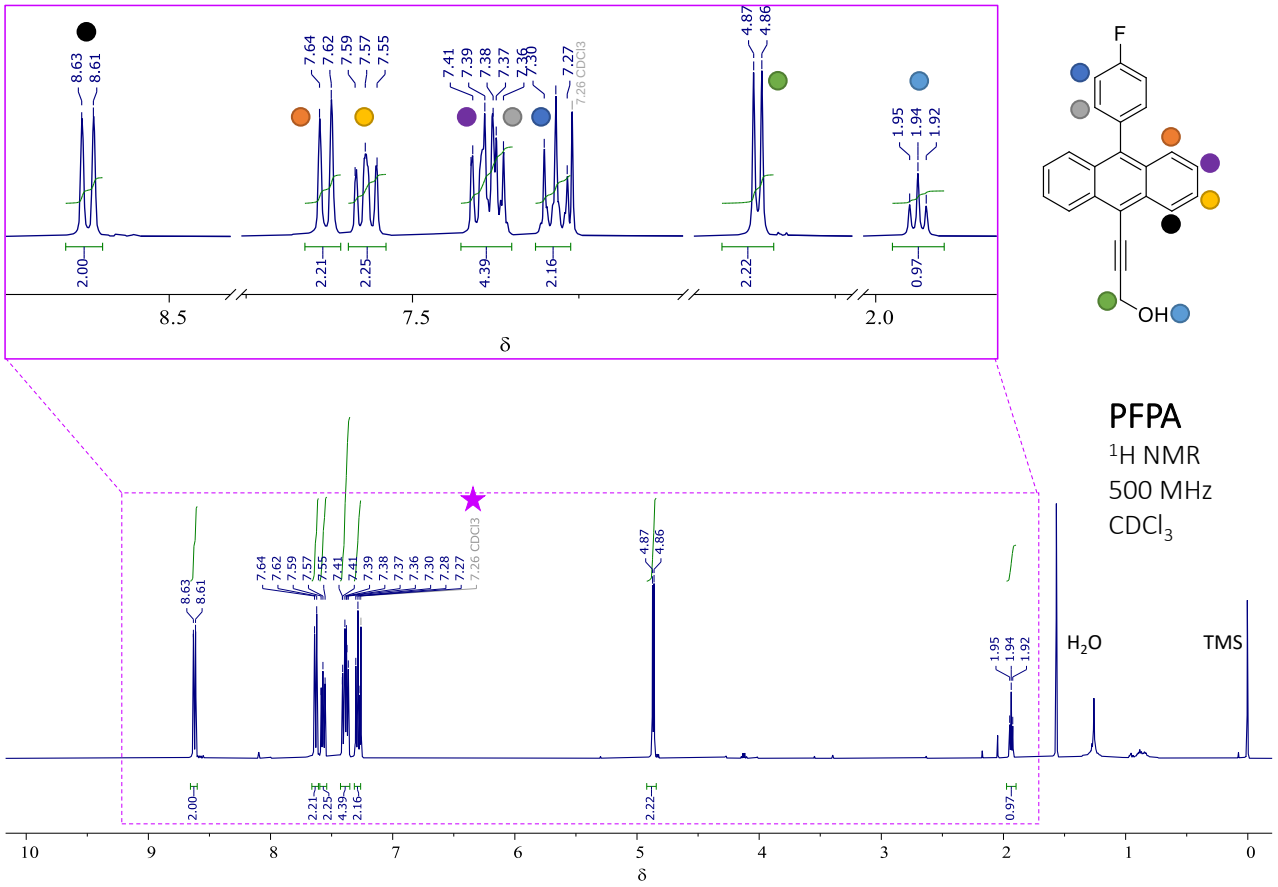
8.63
8.61
7.64
7.62
7.59
7.57
7.55
7.41
7.39
7.38
7.37
7.36
7.30
7.27
7.26 CDCl3
4.87
4.86
1.95
1.94
1.92
2.00
2.21
2.25
4.39
2.16
2.22
0.97
8.5
7.5
2.0
δ
F
OH
PFPA
1H NMR
500 MHz
CDCl3
H2O
TMS
10
9
8
7
6
5
4
3
2
1
0

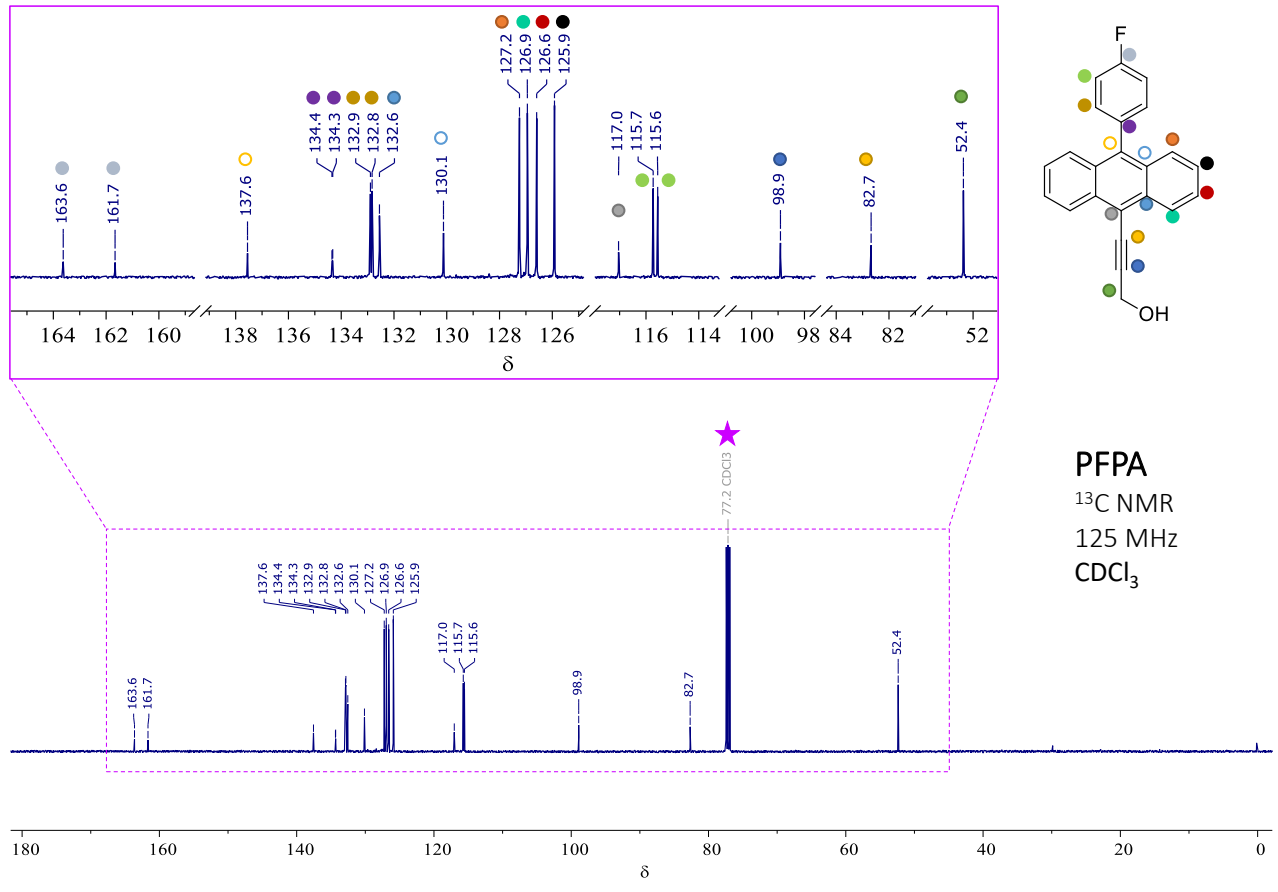
163.6
161.7
137.6
134.4
134.3
132.9
132.8
132.6
130.1
127.2
126.9
126.6
125.9
117.0
115.7
115.6
98.9
82.7
52.4
77.2 CDCl3
164
162
160
138
136
134
132
130
128
126
116
114
100
98
84
82
52
δ
F
OH
PFPA
13C NMR
125 MHz
CDCl3
180
160
140
120
100
80
60
40
20
0

9-(4-methylbenzoic acid)-10-prop-2-yn-1-ol-anthracene (MePCPA)

9-bromo-10-prop-2-yn-1-ol-anthracene (**BPYA**, 0.080 g, 0.26 mmol) was dissolved in freshly distilled THF (3 mL) under vigorous stirring (500 rpm), placed in a round-bottom flask, kept under N_2 atmosphere and heated in an oil bath (T_{set} = 85 °C). 4-(Methoxycarbonyl)phenylboronic acid (mCPBA, 0.038 g, 0.21 mmol), aqueous Cs_2CO_3 (2 M, 0.2 mL, 0.4 mmol) and $Pd(PPh_3)_4$ (0.0108 g, 0.009 mmol) were added together when T_{int} = 40 °C. The mixture resulted in a homogeneous, clear, intense yellow solution. As soon as the reaction started refluxing, it was left to stir for 5 h. After TLC monitoring (*n*-hexane : AcOEt 4 : 1, Rf_{BPYA} = 0.5, Rf_{MePCPA} = 0.4) a second portion of reactants was added to the reaction mix (mCPBA: 0.037 g, 0.21 mmol, Cs_2CO_3 2 M: 0.2 mL, 0.4 mmol, $Pd(PPh_3)_4$: 0.0136 g, 0.012 mmol) and the obtained solution was diluted with more THF (3 mL) and then refluxed overnight for further 16 h.

After TLC monitoring the reaction was stopped. The mixture was cooled to r.t. and the solvent was evaporated to dryness under *vacuum*. The residue was dissolved in ethyl acetate (AcOEt, 10 mL) and washed with brine (10 mL). The aqueous layer was washed with AcOEt (3 x 20 mL) and all the organic fractions were collected and dried over anhydrous Na_2SO_4 for 0.5 h. The solution was filtered on paper before removal of the solvent under *vacuum*. The crude residue (0.097 g) was adsorbed on SiO_2 (0.8 g) and purified by column chromatography on SiO_2 (20 g), eluting with a gradient of solvents from *n*-hexane to *n*-hexane : AcOEt 4 : 1. The final product was obtained after removal of the solvent under *vacuum* (**MePCPA**, 0.053 g, 0.14 mmol, 56 % yield).

^{1}H NMR (500 MHz, $CDCl_3$) δ 8.63 (d, *J* = 7.8 Hz, 2H), 8.26 (d, *J* = 8.6 Hz, 2H), 7.60-7.55 (m, 4H), 7.51 (d, *J* = 8.4 Hz, 2H), 7.39 (ddd, *J* = 8.7, 6.5, 1.3 Hz, 2H), 4.87 (d, *J* = 5.9 Hz, 2H), 4.02 (s, 3H), 1.94 (t, *J* = 6.2 Hz, 1H). **^{13}C NMR (125 MHz, $CDCl_3$)** δ 167.2, 143.7, 137.4, 132.5, 131.5, 129.9, 129.8, 129.6, 127.0, 127.0, 126.7, 126.1, 117.4, 99.1, 82.6, 52.5, 52.4.

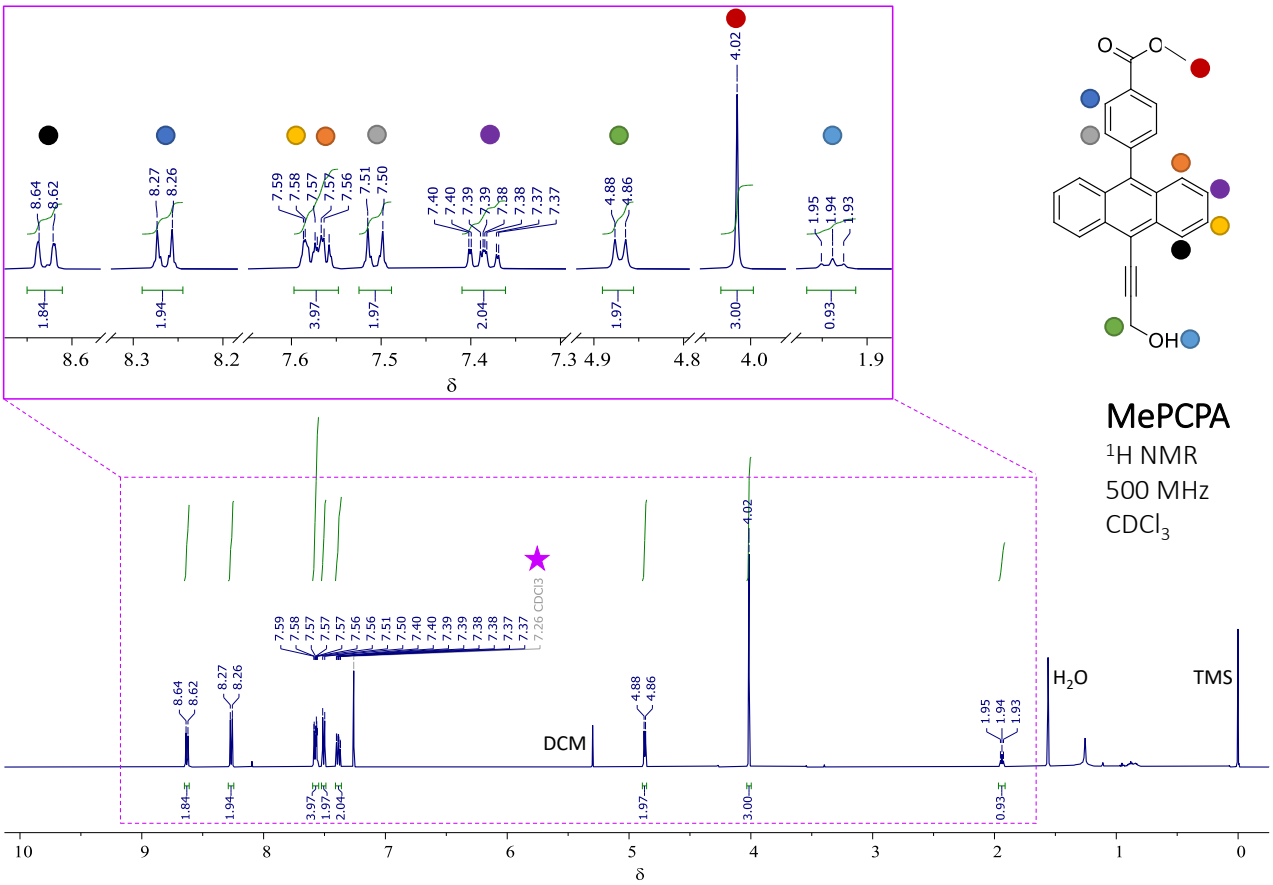
MePCPA
1H NMR
500 MHz
CDCl3
DCM
H2O
TMS
δ

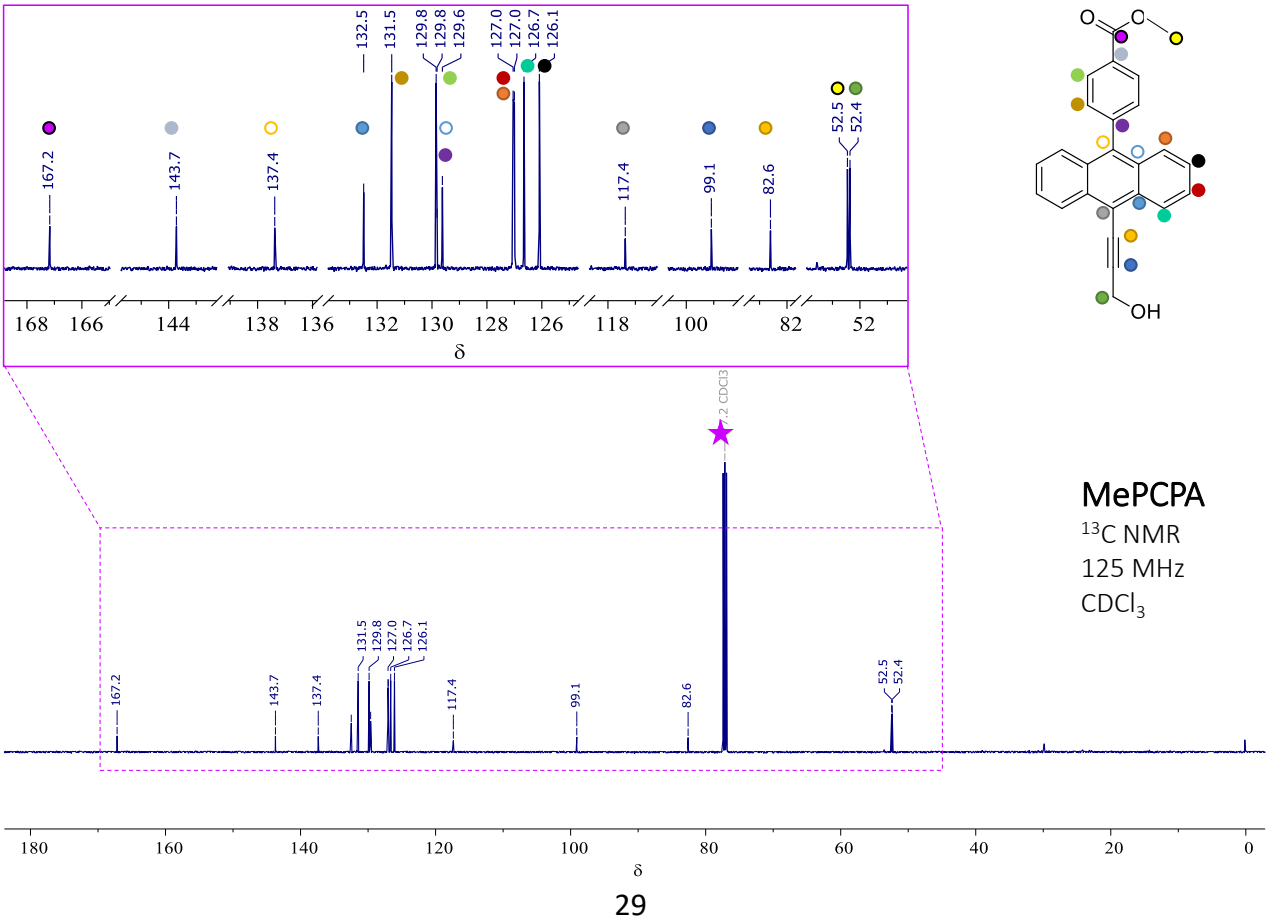
MePCPA
13C NMR
125 MHz
CDCl3
δ

2.4 Methyl deprotection[26]

9-(*para* benzoic acid)-10-prop-2-yn-1-ol-anthracene (PCPA)

A suspension of LiOH (2 M) was prepared in distilled water and sonicated 30 minutes just before use. 9-(4-methylbenzoic acid)-10-prop-2-yn-1-ol-anthracene (**MePCPA**, 0.053 g, 0.14 mmol) was suspended in MeOH (10 mL) under vigorous stirring (500 rpm), placed in a round-bottom flask and heated in an oil bath (T_{set} = 80 °C). The 2 M LiOH suspension (10 mL, 20 mmol) was added to the mixture and the obtained mixture was refluxed for 24 h. After TLC monitoring (*n*-hexane : AcOEt 1 : 1, $Rf_{\mathbf{MePCPA}}$ = 0.5, $Rf_{\mathbf{PCPA}}$ = 0.3), the reaction was cooled at r.t. and the solvent evaporated under *vacuum*. The residue was dissolved in AcOEt (10 mL) and the organic layer was washed with 10% aqueous H_2SO_4 (3 x 5 mL), dried over Na_2SO_4 for 1 hour, filtered on paper and dried under *vacuum*, yielding the final product as dark yellow powder (**PCPA**, 0.030 g, 0.085 mmol, 61 % yield).

^{1}H NMR (500 MHz, DMSO-d_6) δ 12.52 (broad, 1H), 8.60 (d, *J* = 8.8 Hz, 2H), 8.20 (d, *J* = 8.4 Hz, 2H), 7.68 (ddd, *J* = 8.8, 5.5, 2.1 Hz, 2H), 7.57 (d, *J* = 8.4 Hz, 2H), 7.57-7.49 (m, 4H), 5.63 (broad, 1H), 4.68 (broad, 2H). **^{13}C NMR (125 MHz, DMSO-d_6)** δ 167.2, 142.3, 136.6, 131.4, 131.2, 130.4, 129.6, 128.9, 126.9, 126.5, 126.5, 126.4, 117.1, 102.1, 79.8, 50.0. **ESI-MS$^+$**: m/z calc: 352; found: 375 $[PCPA+Na]^+$.

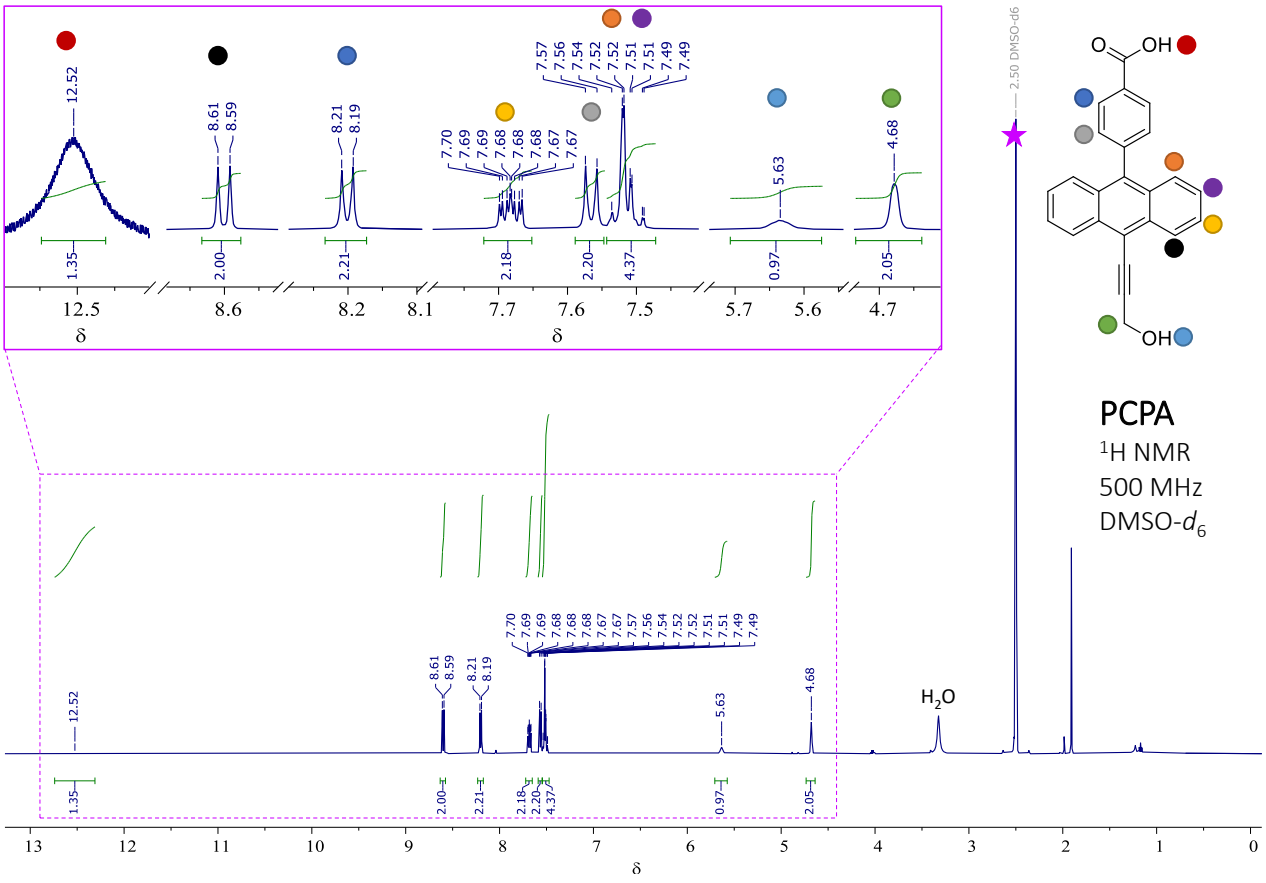
PCPA
^{1}H NMR
500 MHz
DMSO-d_6
H$_2$O
δ

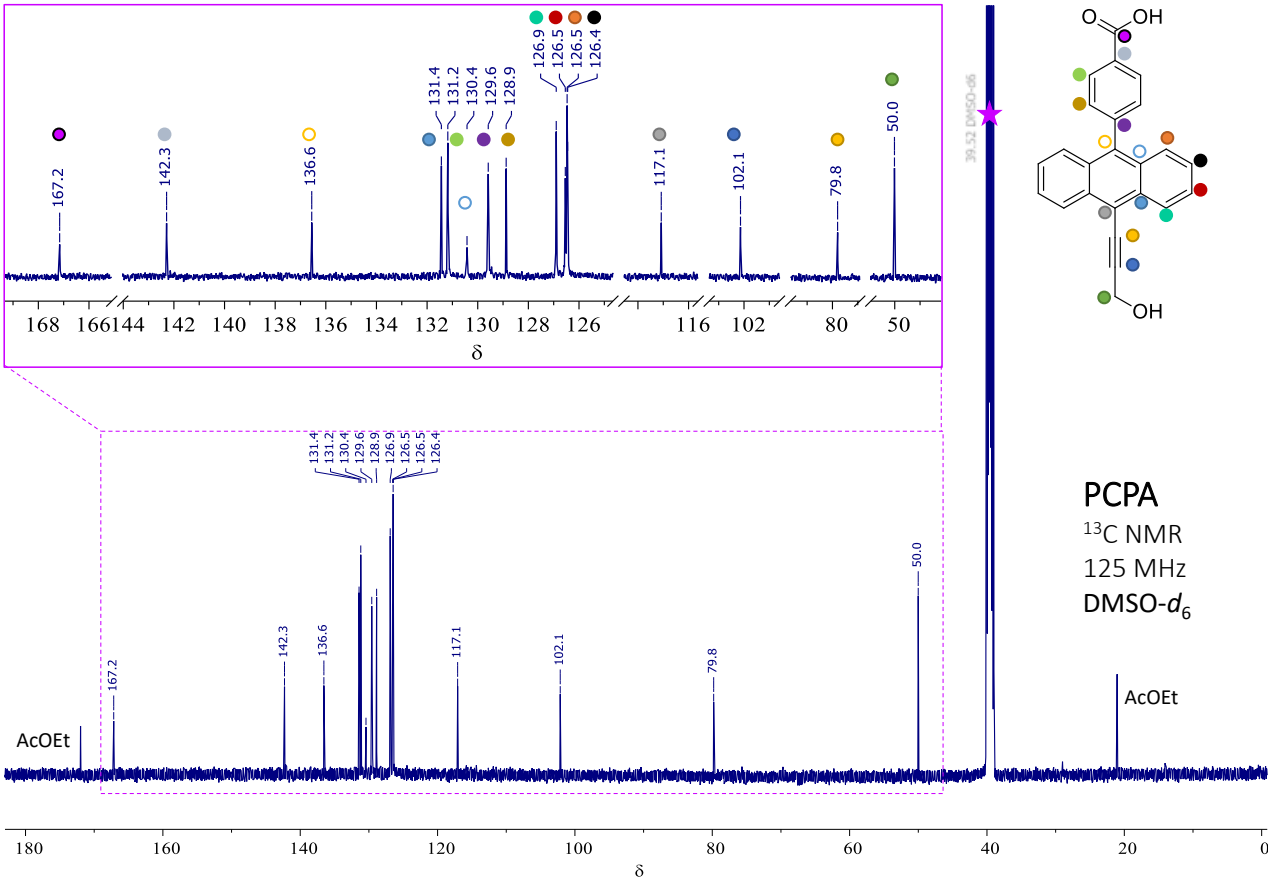
PCPA
^{13}C NMR
125 MHz
DMSO-d_6
AcOEt
δ

2.5 Photochemical step

Synthesys of **PABA-O2**, **DIPA-O2**, **PCPA-O2**, **PFPA-O2**

General procedure. The photooxygenation step was performed on the Vapourtec *Ltd.* easy-Photochem E-Series setup described above in section 1, pag. 2 (Figure S1). Concentrated stock solutions of the anthracene derivatives and the PS were prepared in THF and the final diluted solutions were obtained as a mixture of solvents DCM : THF, 9 : 1 with concentrations of 1 mM for the anthracene substrates and 50 µM for the PS (5% mol/mol). Both solvents were Uvasol®, received from Merck and filtered on basic aluminium oxide (CAS: 1344-28-1, 0.063-0.200 mm, activity stage I, Merck) just before use. The diluted solutions passed through the photochemical reactor (total irradiated volume = 10 mL) using the following parameters:

- LED lamp at 525 nm, 100% intensity
- Flow rate: 0.5 → 5 mL min^{-1} (residence time: 20 → 2 minutes)
- T_{set} = 0 → 25 °C (cooling achieved with a N_2 flux cooled by dry ice)

The reactions were monitored at different time intervals at the spectrophotometer described above (Perkin-Elmer Lambda 950) after transferring the irradiated solution in a 0.1 cm cuvette. The rest of the solution was kept at dark during acquisitions. The irradiated solutions containing EPOs were dried using a C1 Smart Evaporator from BioChromato *Ltd.* at r.t. under *vacuum* for < 12 h. the reaction crudes were stored at -18 °C for max 10 days until O_2 release tests were performed. Only **DIPA-O2** was found not stable enough in these conditions and it was synthesized, concentrated, re-dissolved and tested for O_2 release in the same day.

In order to compare the kinetic of the reaction on different substrates with different absorption profiles, the absorbance values (A) at each time point were converted in: **$A\ \% = (A/A_0) \times 100$**

were A_0 correspond to the maximum value of A, at the beginning of the reaction. These values were always plotted as function of the irradiation time (**Figures S7, S8, S9, S10**).

3,3'-(9,10-dihydro-9,10-epidioxyanthracene-9,10-diyl)bis(prop-2-yn-1-ol) (**DIPA-O2**)

^{1}H NMR (500 MHz, DMSO-d_6) δ 7.76 – 7.69 (m, 4H), 7.48 (dd, *J* = 5.5, 3.2 Hz, 4H), 5.67 (t, *J* = 6.1 Hz, 2H), 4.49 (d, *J* = 6.1 Hz, 4H).

3-(10-(4-fluorophenyl)-9,10-dihydro-9,10-epidioxyanthracen-9-yl)prop-2-yn-1-ol (**PFPA-O2**)

^{1}H NMR (500 MHz, DMSO-d_6) δ 1H NMR (400 MHz, dmso) δ 7.84 – 7.79 (m, 2H), 7.62 (dd, *J* = 9.0, 5.3 Hz, 2H), 7.53 – 7.44 (m, 4H), 7.35 (td, *J* = 7.6, 1.3 Hz, 2H), 7.04 – 6.99 (m, 2H). 5.70 (t, *J* = 6.1 Hz, 1H), 4.53 (d, *J* = 6.2 Hz, 2H).

4-(10-(3-hydroxyprop-1-yn-1-yl)-9,10-dihydro-9,10-epidioxyanthracen-9-yl)benzoic acid (**PCPA-O2**)

^{1}H NMR (500 MHz, DMSO-d_6) δ 8.25 – 8.20 (m, 2H), 7.82 (dd, *J* = 7.5, 1.3 Hz, 1H), 7.73 – 7.68 (m, 2H), 7.48 (td, *J* = 7.5, 1.1 Hz, 2H), 7.35 (td, *J* = 7.6, 1.4 Hz, 2H), 7.01 (d, *J* = 7.4 Hz, 2H), 5.70 (t, *J* = 6.1 Hz, 1H), 4.53 (d, *J* = 6.1 Hz, 2H).

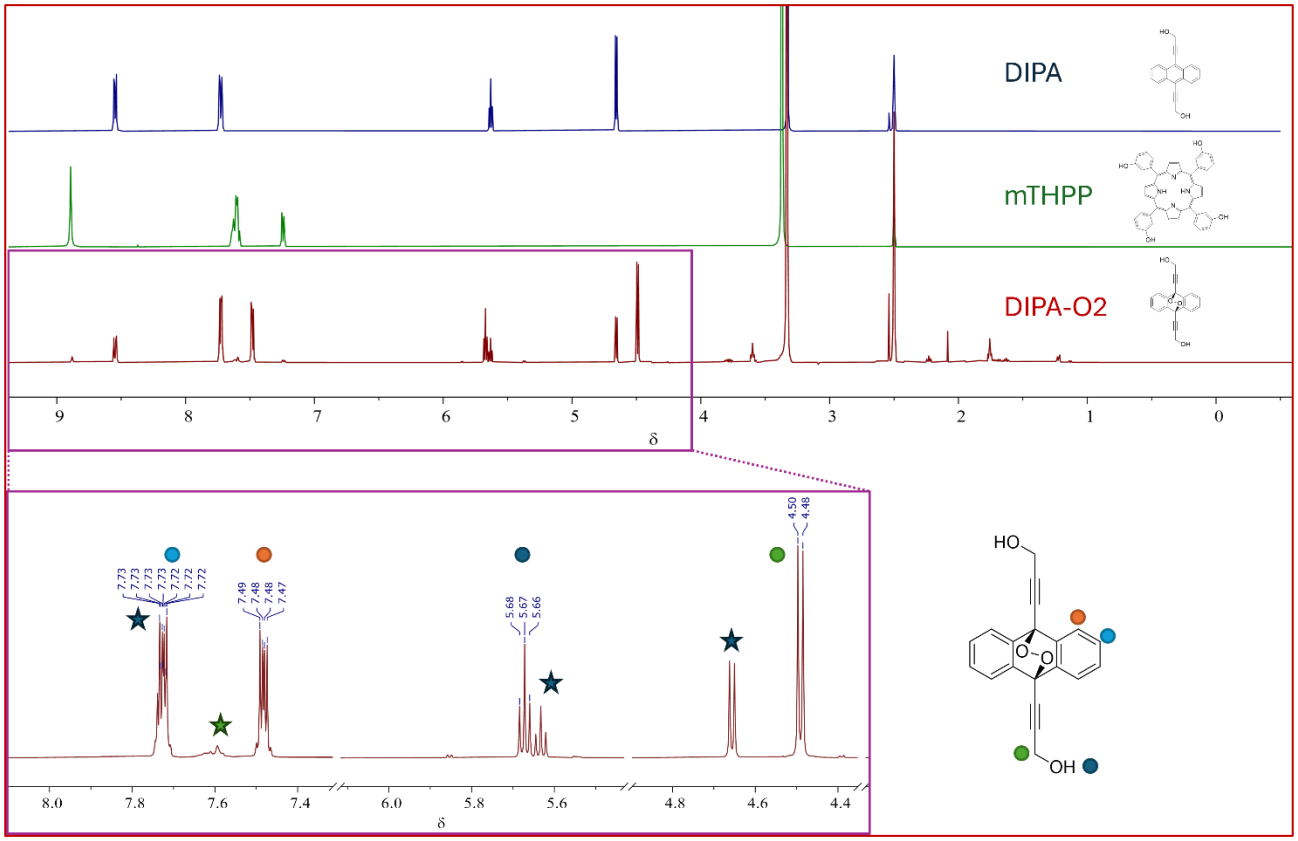

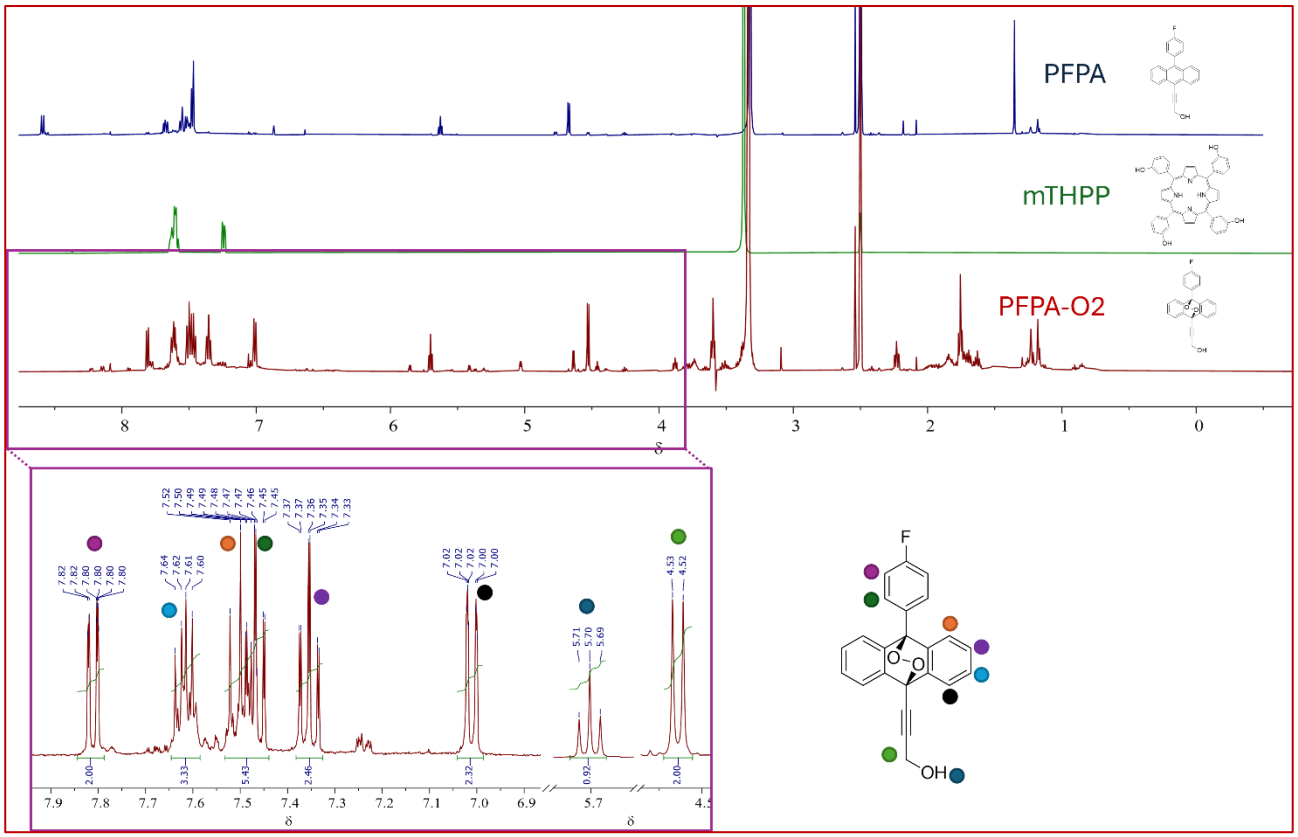
PFPA
mTHPP
PFPA-O2
F
O
O
OH

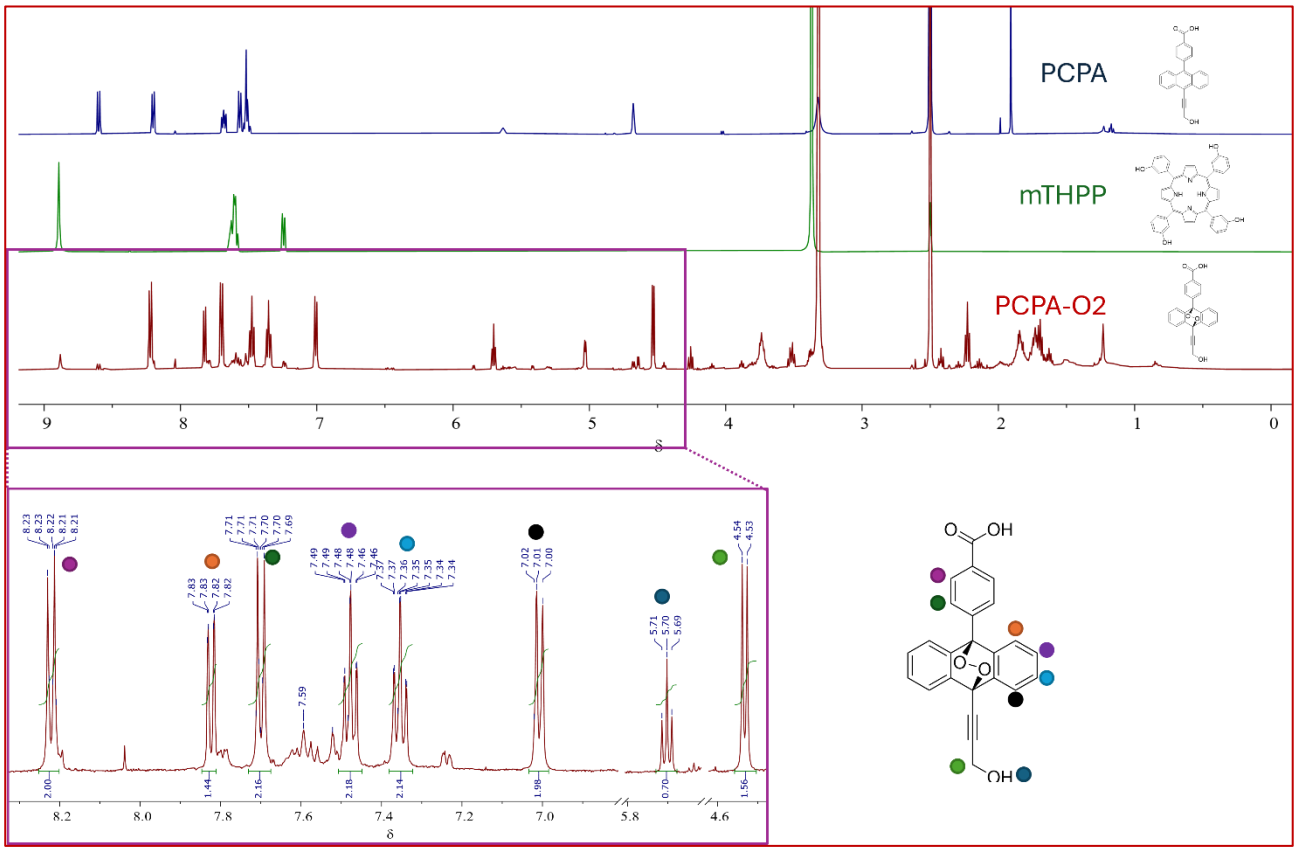
PCPA
mTHPP
PCPA-O2
O
OH
O
O
OH

2.6 Cycloreversion

Release of molecular oxygen from **PABA-O2**, **DIPA-O2**, **PCPA-O2**, **PFPA-O2**

General procedure. The cycloreversion of synthesized EPOs was performed on the reaction crudes obtained after evaporation of the solvents. The solid residues were dissolved in 1 mL of DMSO-d_6 obtaining a concentration of EPOs = 6 mM and PS = 300 µM. These solutions were divided as follows:

- 600 µL were transferred into NMR tubes: a series of ^{1}H NMR spectra were acquired (400 or 500 MHz, 298K) just upon dissolution and after storage in thermostated water bath.
- 400 µL were further diluted with DMSO Uvasol® to a final concentration of EPOs = 200 µM and PS = 10 µM. Three samples were used in 3 different 1 x 1 cm quartz cuvettes equipped with magnetic bars and the absorption spectra revealing the kinetic of O_2 release were acquired on the Agilent Cary 100 UV-Vis spectrophotometer described above at 25 °C, 37.5 °C and 50 °C. Scanning kinetics of 30 minutes were used and spectra cycles in the range 200-450 nm were completed every 2 minutes (total of 16 spectra per run).

4. References

[1] M. J. Frisch, G. W. Trucks, H. B. Schlegel, G. E. Scuseria, M. A. Robb, J. R. Cheeseman, G. Scalmani, V. Barone, G. A. Petersson, H. Nakatsuji, X. Li, M. Caricato, A. V Marenich, J. Bloino, B. G. Janesko, R. Gomperts, B. Mennucci, H. P. Hratchian, J. V Ortiz, A. F. Izmaylov, J. L. Sonnenberg, D. Williams-Yung, F. Ding, F. Lipparini, F. Egidi, J. Goings, B. Peng, A. Petrone, T. Henderson, D. Ranasinghe, V. G. Zakrzewski, J. Gao, N. Rega, G. Zheng, W. Liang, M. Hada, M. Ehara, K. Toyota, R. Fukuda, J. Hasegawa, M. Ishida, T. Nakajima, Y. Honda, O. Kitao, H. Nakai, T. Vreven, K. Throssell, J. A. Montgomery Jr., J. E. Peralta, F. Ogliaro, M. Bearpark, J. J. Heyd, E. Brothers, K. N. Kudin, V. N. Staroverov, T. A. Keith, R. Kobayashi, J. Normand, K. Raghavachari, A. Rendell, J. C. Burant, S. S. Iyengar, J. Tomasi, M. Cossi, J. M. Millam, M. Klene, C. Adamo, R. Cammi, J. W. Ochterski, R. L. Martin, K. Morokuma, O. Farkas, J. B. Foresman, D. J. Fox, *Gaussian 16 Revis. A 03* **2016**.

[2] C. Lee, W. Yang, R. G. Parr, *Phys. Rev. B* **1988**, *37*, 785–789.

[3] S. H. Vosko, L. Wilk, M. Nusair, *Can. J. Phys.* **1980**, *58*, 1200–1211.

[4] P. J. Stephens, F. J. Devlin, C. F. Chabalowski, M. J. Frisch, *J. Phys. Chem.* **1994**, *98*, 11623–11627.

[5] A. D. Becke, *J. Chem. Phys.* **1993**, *98*, 5648–5652.

[6] F. Weigend, *Phys. Chem. Chem. Phys.* **2006**, *8*, 1057–1065.

[7] F. Weigend, R. Ahlrichs, *Phys. Chem. Chem. Phys.* **2005**, *7*, 3297–3305.

[8] W. Fudickar, T. Linker, *J. Phys. Org. Chem.* **2019**, *32*, e3951.

[9] Y.-Q. He, W. Fudickar, J.-H. Tang, H. Wang, X. Li, J. Han, Z. Wang, M. Liu, Y.-W. Zhong, T. Linker, P. J. Stang, *J. Am. Chem. Soc.* **2020**, *142*, 2601–2608.

[10] A. Putta, A. G. Sykes, H. Sun, *J. Fluor. Chem.* **2020**, *235*, 109548.

[11] D. Lovison, D. Alessi, L. Allegri, F. Baldan, M. Ballico, G. Damante, M. Galasso, D. Guardavaccaro, S. Ruggieri, A. Melchior, D. Veclani, C. Nardon, W. Baratta, *Chem. – A Eur. J.* **2022**, *28*, e202200200.

[12] M.-P. Minadakis, K. F. Mavreas, D. D. Neofytos, M. Paschou, A. Kogkaki, V. Athanasiou, M. Mamais, D. Veclani, H. Iatrou, A. Venturini, E. D. Chrysina, P. Papazafiri, T. Gimisis, *Org. Biomol. Chem.* **2022**, *20*, 2407–2423.

[13] B. Ventura, D. Veclani, A. Venturini, N. Armaroli, M. Baroncini, P. Ceroni, M. Marchini, *Chem. – A Eur. J.* **2023**, *29*, e202301853.

[14] B. Mennucci, J. Tomasi, R. Cammi, J. R. Cheeseman, M. J. Frisch, F. J. Devlin, S. Gabriel, P. J. Stephens, *J. Phys. Chem. A* **2002**, *106*, 6102–6113.

[15] S. F. Boys, F. Bernardi, *Mol. Phys.* **1970**, *19*, 553–566.

[16] E. R. Johnson, S. Keinan, P. Mori-Sánchez, J. Contreras-García, A. J. Cohen, W. Yang, *J. Am. Chem. Soc.* **2010**, *132*, 6498–6506.

[17] J. Contreras-García, E. R. Johnson, S. Keinan, R. Chaudret, J.-P. Piquemal, D. N. Beratan, W. Yang, *J. Chem. Theory Comput.* **2011**, *7*, 625–632.

[18] C. F. R. A. C. Lima, L. R. Gomes, L. M. N. B. F. Santos, J. N. Low, *Acta Crystallogr. Sect. E Struct. Reports Online* **2009**, *65*, o3037–o3037.

[19] M. (WI) APEX3 Software Package V2019, Bruker AXS Inc., **2019**.

[20] M. (WI) Bruker SAINT, v8.40A: Part of the APEX3 Software Package V2019, Bruker AXS Inc., **2019**.

[21] M. (WI) Bruker SADABS V2016/2: Part of the APEX3 Software Package V2019, Bruker AXS Inc., **2019**.

[22] G. M. Sheldrick, *Acta Crystallogr. Sect. A, Found. Adv.* **2015**, *71*, 3–8.

[23] G. M. Sheldrick, *Acta Crystallogr. Sect. C* **2015**, *71*, 3–8.

[24] A. L. Spek, *Acta Crystallogr. Sect. C* **2015**, *71*, 9–18.

[25] C. F. Macrae, I. Sovago, S. J. Cottrell, P. T. A. Galek, P. McCabe, E. Pidcock, M. Platings, G. P. Shields, J. S. Stevens, M. Towler, P. A. Wood, *J. Appl. Crystallogr.* **2020**, *53*, 226–235.

[26] M. Agnes, A. Mazza, E. Kalydi, S. Béni, M. Malanga, I. Manet, *Chem. - A Eur. J.* **2023**, *29*, DOI 10.1002/chem.202300511.

[27] W. Fudickar, T. Linker, *Chem. - A Eur. J.* **2011**, *17*, 13661–13664.

[28] W. Fudickar, T. Linker, *J. Am. Chem. Soc.* **2012**, *134*, 15071–15082.